Industrial Chemistry & Materials

ROYAL SOCIETY
OF **CHEMISTRY**

ICM
Industrial Chemistry & Materials

Check for updates

Progress on aqueous rechargeable aluminium metal batteries

Xiaotian Wang,† Zihang Xi† and Qing Zhao iD *

Aqueous rechargeable aluminium metal batteries (ARAMBs) have advantages of high energy density, cost efficiency and reasonable safety. However, parasitic reactions between the Al anode and electrolyte, sluggish dynamics and low reversibility of the Al anode, and structural instability caused by the high charge density of Al^{3+} ions lead to a short cycling life and inferior high-rate performance in ARAMBs. Herein, in this review, we summarize the research progress on ARAMBs by emphasizing the reported strategies to address the above-mentioned intractable issues. Initially, we discuss how to regulate the Al anode and interphase to accelerate the kinetics of Al stripping, which mainly includes strategies of ionic liquid analogue-derived solid electrolyte interphases (SEIs), artificial interfacial functional layer and aluminium alloy. Subsequently, the electrolyte modification approaches are highlighted including preparing highly concentrated single-salt/bi-salt electrolytes and designing electrolyte additives to reduce the parasitic reactions of ARAMBs. Finally, we introduce the progress on fabricating cathodes, such as vanadium-based materials, manganese-oxide materials, molybdenum-based materials, Prussian blue analogues, carbon materials, and organic materials to accommodate Al^{3+} ions. We propose that the further development of ARAMBs requires the cooperation of the above-mentioned strategies to improve their overall electrochemical performance and the development of new methods to illustrate the reaction mechanism of batteries.

Keywords: Aqueous batteries; Interphase design; Al anode; Electrolyte modification; Cathode materials.

State Key Laboratory of Advanced Chemical Power Sources, Frontiers Science Center for New Organic Matter, Key Laboratory of Advanced Energy Materials Chemistry (Ministry of Education), College of Chemistry, Nankai University, Tianjin 300071, China. E-mail: zhaoq@nankai.edu.cn
† These authors contributed equally to this work.

1 Introduction

Given that the non-renewable traditional fossil energy cannot satisfy the long-term demands for energy consumption, environmentally friendly renewable energy sources are gaining increasing prominence in energy supply.[1,2] However, these sustainable energy sources such as solar and wind energy are constrained by natural conditions with uneven temporal and spatial distribution, which highlights the

Xiaotian Wang is currently pursuing his Ph.D. in Inorganic Chemistry at Nankai University under the supervision of Prof. Qing Zhao. He received his B.S. in Chemistry at Nankai University in 2023. His research interests are focused on the design and preparation of electrolytes for aqueous rechargeable aluminum metal batteries.

Xiaotian Wang

Zihang Xi is currently pursuing his M.S. in Inorganic Chemistry at Nankai University under the supervision of Prof. Qing Zhao. He received his B.S. in Chemistry at Nankai University in 2023. His research interest focuses on the design of electrolyte additives for aqueous rechargeable aluminum metal batteries.

Zihang Xi

importance of developing large-scale energy storage systems (ESSs).[3,4] As one of the most successful electrochemical ESSs, lithium-ion batteries (LIBs), which have advantages of less space restriction, higher conversion efficiency/energy density, faster response speed and shorter construction time than pumped storage, have witnessed rapid development in recent years.[5] However, the limited/uneven distribution of lithium resources and the safety risk associated with LIBs limit their application in large-scale energy storage.[6] Accordingly, significant efforts have been devoted to developing adequate alternatives beyond lithium batteries, such as sodium, potassium, zinc, magnesium, calcium, and aluminium batteries.[7] Among them, sodium-ion batteries (NIBs) have been the most widely studied due to the highly abundant Na resource and their similar working principle with LIBs.[8,9] Nevertheless, given that flammable organic electrolytes are used in NIBs, their safety is still an issue especially considering the huge electrical energy in ESSs. Therefore, the development of intrinsically safe electrochemical ESSs is urgent.

Rechargeable batteries that operate under the condition of aqueous electrolyte are emerging as potential EESs with merits of high safety and low cost.[10,11] Moreover, when using metallic zinc and aluminium as anodes that exhibit low reactivity in the atmosphere and moisture, the constructed aqueous rechargeable batteries can also deliver a high energy density (Fig. 1).[12–15] Compared with zinc batteries, aluminium metal batteries (AMBs) show the following merits: 1) high abundance in the Earth's crust (8.21 wt% for Al and 0.0076 wt% for zinc). 2) Large-scale production with low cost. 3) Potential three-electron transfer mechanism with lightweight characteristic allows aluminium metal to achieve extremely high specific capacities (2980 mA h g^{-1} and 8046 mA h cm^{-3} for Al, 820 mA h g^{-1} and 5855 mA h cm^{-3} for zinc).

Although aluminium was reported as a battery anode in the Buff battery as early as 1857 and other primary Al batteries such as Al/air, Al/sulphur, and Al/CO$_2$ batteries are also well known, the first rechargeable aluminium battery only appeared in 2011, when Archer *et al.* applied AlCl$_3$/1-ethyl-3-methylimidazolium chloride ([EMIm]Cl) ionic liquid (IL) electrolyte to achieve the reversible operation of an Al/V$_2$O$_5$ battery.[17–23] However, due to the sluggish kinetics and less reversible electrochemistry of the V$_2$O$_5$ cathode, the development of AMBs was still slow until anion intercalation chemistry was found in the graphite cathode in 2015.[24] The Al/graphite battery using the AlCl$_3$-[EMIm]Cl IL electrolyte exhibits fast kinetics with an excellent cycling performance (over 7000 charge/discharge cycles), boosting the development of this emerging ESS.[24–26] Various cathode materials such as organic compounds, carbon materials, metal chalcogenide, sulphur, metal–organic frameworks and aluminium anode host/current collectors have been reported for AMBs with an increased specific capacity and cycling life.[27–38]

However, despite the merits of IL-based aluminium batteries, the moisture sensitivity of IL makes it difficult to assemble AMBs under atmospheric conditions, thus greatly increasing the production costs and contradicting the advantages of aluminium-metal anodes.[39,40] Meanwhile, due to the large anion (AlCl$_4^-$) interaction mechanism, the cathode has a low specific capacity (usually less than 100 mA h g^{-1}).[35,41] In comparison, aqueous rechargeable aluminium metal batteries (ARAMBs) using metallic Al as the anode and high-safety aqueous electrolytes have emerged as potential candidates in last five years. However, although the high specific capacity and moderate redox potential of Al^{3+}/Al result in a high theoretical energy density in ARAMBs, there are still intractable issues that need to be overcome before their commercial application. Currently, the most prominent problem associated with ARAMBs is the interface between the aluminium-metal anode and the aqueous electrolyte, which is not present in aqueous Al-ion batteries.[42–47] Furthermore, due to the low standard reduction potential of Al (−1.676 V *vs.* standard hydrogen electrode, SHE), the hydrogen evolution reaction (HER) theoretically occurs prior to the electrochemical stripping of Al.[17] Although a dense passivated oxide layer with large band gap can suppress the spontaneous HER, it also significantly reduces the reaction kinetics of the Al anode.[48] Moreover, the easy passivation of the oxide layer also prevents the reversible stripping/deposition of aluminium. Meanwhile, the high charge density of Al^{3+} ions also leads to a strong electrostatic interaction with the cathode material, which predisposes the cathode to structural disintegration, and thus reduces the battery capacity.[49]

Thus, to overcome the issues associated with ARAMBs, considerable efforts have been devoted to designing anode, electrolyte and cathode materials in last five years (Fig. 2). The rapid increase in the number of publications and the inconsistent conclusions from various works make a review in this field necessary. Herein, we focus on the research progress on ARAMBs that operate under aqueous electrolyte conditions. This review summarizes the modification strategies in terms of three aspects, including Al anode and interphase regulation, modification of aqueous electrolytes,

Qing Zhao received his B.S. (2012) and Ph.D. (2017) degrees from Nankai University. He was a Postdoctoral Fellow in Cornell University from 2017 to 2021. Presently, he is a Professor in Nankai University. His research interests focus on the interphase chemistry of electrode/electrolyte and advanced battery systems.
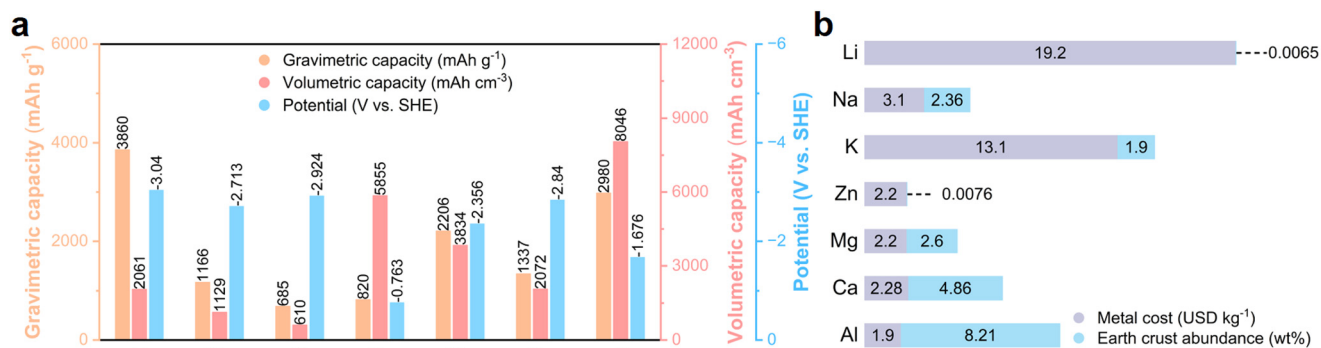
Qing Zhao

Fig. 1 Advantages of Al as a battery anode. (a) Comparison of theoretical specific capacities and standard electrochemical reduction potentials of different metal anodes. (b) Abundance of different metal elements in the Earth's crust and the cost of metal anodes. Reprinted with permission.[16] Copyright 2021, WILEY-VCH VERLAG GMBH.

and design of cathode materials. On the anode side, we emphasize that the modification of Al metal anodes and electrolytes needs collaboration to stabilize the operation of batteries. On the cathode side, the storage mechanism is still ambiguous for most cathode materials given that various ions such as Al^{3+}, H^+, $Al(CF_3SO_3)^{2+}$, and $AlCl_4^-$ have been reported as charge carriers in ARAMBs. We anticipate that this review can offer fundamental principles for designing advanced electrodes and electrolytes for next-generation energy-dense aqueous batteries.

2 Al anode and interphase regulation

It is difficult for pure Al metal to function as an anode in conventional aqueous electrolytes owing to the sluggish Al stripping process caused by the passivation film on the

Fig. 2 Modification strategies for aqueous rechargeable Al metal batteries.

surface of Al and inevitable HER once fresh Al is exposed to the electrolyte. Thus, to alleviate the above-mentioned issues, it is necessary to modify the interface of Al to inhibit interface passivation and side reactions towards the electrolyte. To date, a few strategies have been proposed to modify the aluminium metal anode, which can be generally summarized as ionic liquid analogue-derived solid electrolyte interphase (SEI), artificial interfacial functional layer, and aluminium alloy anode.

2.1 Ionic liquid analogue-derived SEI

A qualified SEI that is endowed with electronic insulation and ionic conductivity has been well known for enabling reversible stripping/plating of alkali metal anodes.[50] In 2018, Zhao *et al.* proposed a strategy to construct an SEI on an Al anode by pre-treating aluminium foil with an AlCl$_3$-[EMIm]Cl IL electrolyte.[48] The IL could erode the Al_2O_3 passivation film of Al by forming a new interfacial layer rich in IL derivatives, which contained abundant C≡N, C≡O, and C≡C bonds according to the FTIR spectra (Fig. 3a). In comparison, the vibration modes of the imidazolium ring in [EMIm]Cl largely disappeared, indicating that imidazolium may undergo ring-open reactions on the surface of Al, preventing the oxidation of the Al anode. The IL-derived SEI effectively transformed the interfacial chemistry of the metal anode (Fig. 3b and c), enabling fast charge transport at the electrolyte/electrode interface. Since then, more works using Al anodes modified by ionic liquids have been reported to match various cathode materials, such as Prussian blue analogues (PBAs), organic materials, carbon materials and transition metal oxides.[49,51–55] Besides the expensive IL-based electrolytes, some low-cost eutectic solvents can also be used to pre-treat Al metal anodes. For example, the AlCl$_3$–acetamide deep eutectic solution (DES, AlCl$_3$/Acm = 1.3 by molar ratio) can also erode the passivation layer of aluminium metal anodes.[56] The difference in the surface chemical composition of Al anodes before and after treatment with DES was characterized by XPS tests (Fig. 3d and e, respectively), which showed a significant reduction in oxides and the appearance
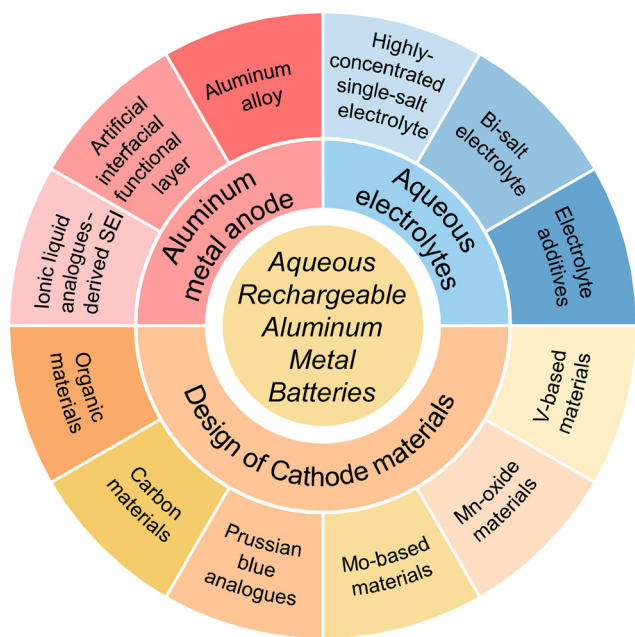
© 2025 The Author(s). Co-published by the Institute of Process Engineering, Chinese Academy of Sciences and the Royal Society of Chemistry

Ind. Chem. Mater., 2025, **3**, 7–30 | 9

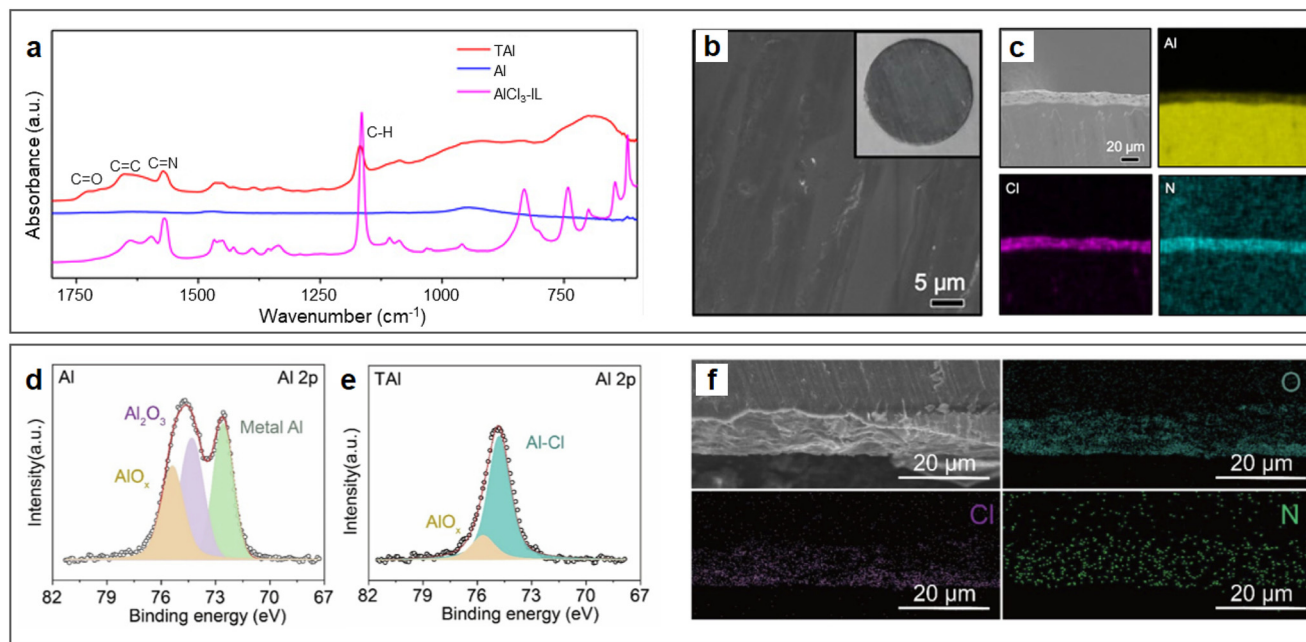**Fig. 3** Characterization of ionic liquid analogue-derived SEI. (a–c) $AlCl_3$-[EMIm]Cl ionic liquid electrolyte-treated Al (TAl) foil. (a) Attenuated total reflection-Fourier transform infrared spectra (ATR-FTIR) of Al and TAl foil. SEM images of (b) surface with inserted digital photo and (c) cross-section with corresponding EDS mapping of Al, Cl, and N of TAl foil. Reproduced with permission.[48] Copyright 2018, AMER ASSOC ADVANCEMENT SCIENCE. (d–f) $AlCl_3$–acetamide deep eutectic solution-treated Al (TAl) foil. X-ray photoelectron spectra (XPS) of Al 2p on the surface of (d) Al foil and (e) TAl foil. (f) Cross-sectional SEM image and corresponding EDS mapping of O, Cl and N of TAl foil. Reproduced with permission.[56] Copyright 2021, ELSEVIER.

of a new peak corresponding to Al–Cl bonds, demonstrating that the interfacial chemistry of the metal anode was effectively transformed. This conclusion was also be supported by the cross-section scanning electron microscopy (SEM) images and energy-dispersive X-ray spectroscopy (EDS) (Fig. 3f), where the interphase was rich in Cl, O, and N. Overall, the SEI on the Al anode generated by eutectic electrolytes can largely improve the kinetics of the Al stripping process. In general, organic cations in ionic liquid analogues undergo chemical transformation on the surface of the Al anode. In addition, the residual $AlCl_3$ analogue provides an acidic environment for fast charge transfer kinetics.

Although the stripping/plating kinetics of the Al anode can be significantly accelerated, the long-term stability of the ionic liquid analogue-derived SEI in aqueous electrolyte has been questioned.[57] After immersing the IL-derived SEI in highly concentrated $Al(CF_3SO_3)_3$ $(Al(OTF)_3)$ aqueous electrolyte for 30 min, it underwent drastic changes (Fig. 4a). Subsequently, the XPS Al 2p spectra, which were previously dominated by a single $AlCl_3$ peak, exhibited various peaks including Al metal, oxides, hydroxides and AlF_3. The chronopotentiometry results indicated that although the IL-treated Al anodes possessed lower "overpotentials" for each half-reaction compared with the pure Al anodes, their superior electrochemical activity was significantly reduced upon prolonged immersion in aqueous electrolyte. This phenomenon was also observed in a urea-$AlCl_3$ eutectic

solvent-derived SEI.[58] After exposing the Al anode treated by urea-$AlCl_3$ eutectic solvent (UTAl) to air for 48 h, the XPS Al 2p spectra showed that its surface was still covered by chloride salts of Al (Fig. 4b). However, the presence of Al-based fluoride salt and an increase in the relative amount of Al oxide on the surface of UTAl were observed after the first stripping (Fig. 4c), indicating that the partial rupture and dissolution of the SEI may occur in aqueous electrolytes.

Overall, the construction of SEIs for aluminium anodes *via* ionic liquid analogues can significantly enhance the charge transport kinetics at the anode/electrolyte interface, particularly in symmetric batteries, showing a large reduction in voltage hysteresis compared to pure aluminium anodes under galvanostatic tests. However, the stability of SEIs constructed by this strategy in the atmospheric environment as well as in aqueous electrolytes has been questioned. There are few reports demonstrating the Coulombic efficiencies (CE) of aluminium metal stripping/deposition, and there is also a lack of studies exploring the associated reaction mechanisms.

2.2 Artificial interfacial functional layer

Various strategies have been developed for constructing stable artificial interfacial functional layers on the surface of aluminium metal anodes. Among them, the poly(vinylidene difluoride) (PVDF) coating prepared by the spin coating method not only prevented water and oxygen infiltration but
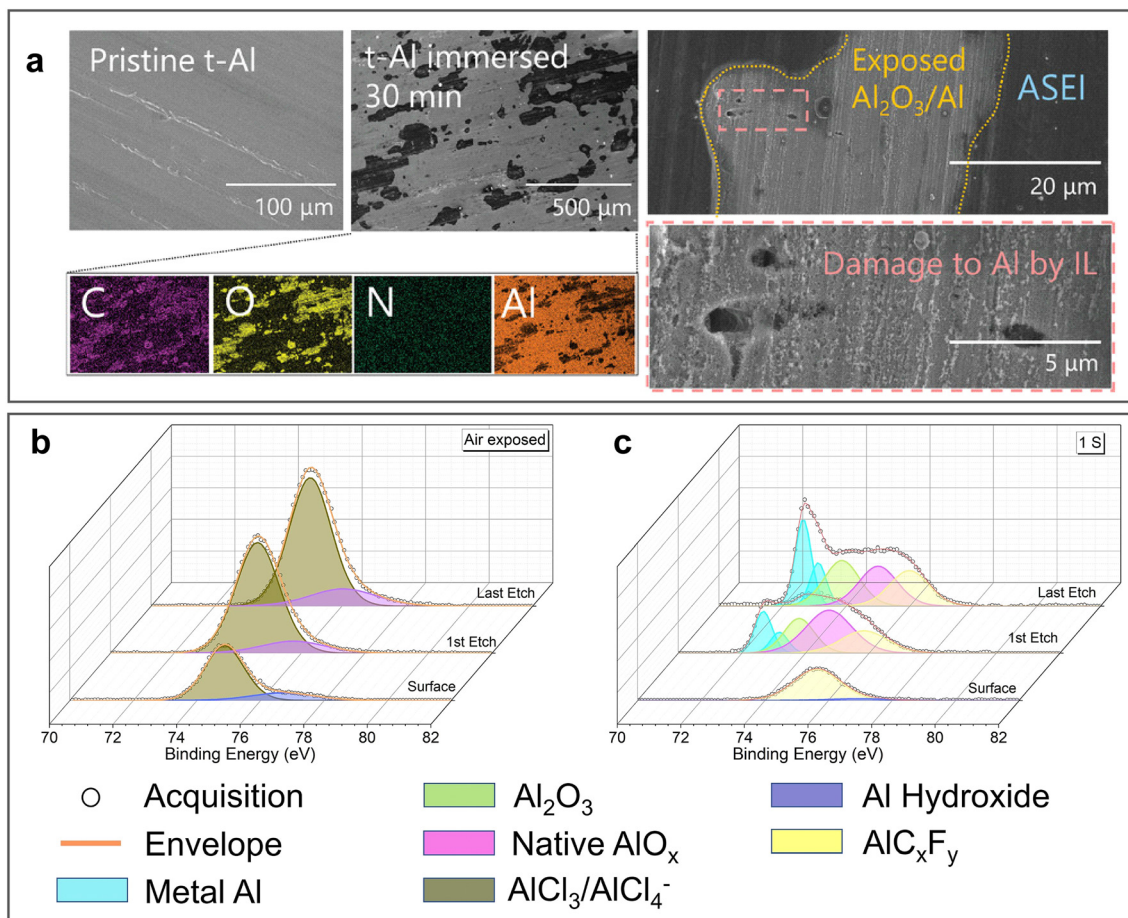
Fig. 4 Long-term stability of ionic liquid analogue-derived SEI. (a) SEM images and corresponding EDX mapping of TAl foil before and after immersion in 5 M Al(OTF)$_3$ electrolyte (left). The magnified image on the right shows the damage of SEI. Reproduced with permission.[57] Copyright 2021, WILEY-VCH VERLAG GMBH; Al 2p XPS spectra of UTAl foil (b) after 48 h of exposure to air and (c) after a round of stripping in a symmetric cell. Reproduced with permission.[58] Copyright 2022, ELSEVIER SCIENCE SA.

also had the function of guiding the deposition of Al^{3+} ions on the electrode.[59] The working mechanism of the bifunctional PVDF coating can be briefly described as follows: β-PVDF with all-trans structure enabled the strong interaction through the F–Al bond, and thus guided the deposition of Al^{3+} on the electrode. In addition, the hydrophobic nature of the PVDF coating hindered the contact between the bare Al and free H$_2$O, which inhibited the HER (Fig. 5a). The linear polarization curves of PVDF-Al and bare Al showed that the corrosion current of PVDF-Al (1.31 mA cm^{-2}) was lower than that of bare Al (1.78 mA cm^{-2}), which indicated the slower corrosion rate of the PVDF-Al electrode (Fig. 5b). The linear sweep voltammetry (LSV) studies indicated that PVDF-Al showed a lower initial HER potential of 0.08 V (vs. Al/Al^{3+}) than that of the bare Al anode (0.51 V vs. Al/Al^{3+}) (Fig. 5c). The amorphization strategy has also been applied for the construction of an interfacial functional layer on the surface of aluminium metal anodes. Yan et al. first constructed a porous amorphous metallic Al functional layer on the surface of an aluminium substrate (Al@a–Al) via an in situ lithiation/delithiation method, and further coated a polymer film to increase the overpotential of HER (Fig. 5d).[60] The amorphous

Al structure endowed the Al anode with the merits of low Al nucleation energy barrier and fast interfacial ions transfer kinetics. The electrochemically active surface area-normalized corrosion current density of Al@a–Al was about 400 times lower than that of bare Al (Fig. 5e), which confirmed the intrinsically restrained self-corrosion of Al@a–Al compared with bare Al. Meanwhile, the LSV studies indicated that the polymer film facilitated a markedly widened cathodic limit (Fig. 5f), ensuring the stable and reversible aluminium stripping/plating in the Al@a–Al@polymer anode. In addition, artificial interfacial functional layers can also be constructed on the surface of aluminium alloy anodes to improve the reversibility of ARAMBs. A eutectic aluminium–cerium alloy uniformly grafted with ultrathin MXene (MXene/E-Al$_{97}$Ce$_3$) was reported as a highly flexible, reversible, and dendrite-free anode for ARAMBs (Fig. 5g).[61] In the composite anode, the grafted ultrathin MXene layer not only suppressed the Al corrosion behaviour (Fig. 5h), but also alleviated the passivating effect of the native oxide layer to facilitate Al^{3+} transport, resulting in a significant enhancement of Al stripping/plating behaviour. Furthermore, no gas bubbles were observed at the MXene/E-Al$_{97}$Ce$_3$ electrode due to the
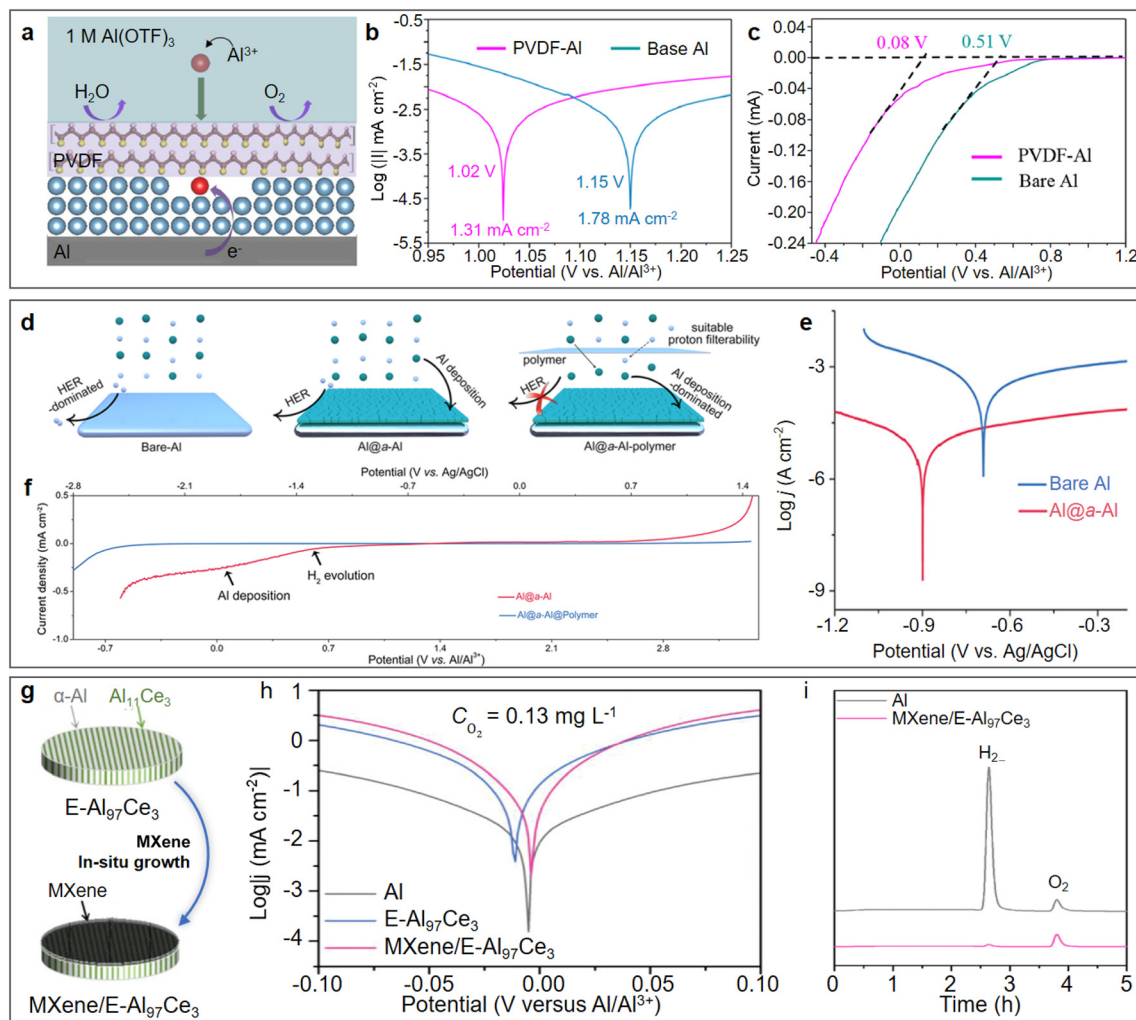
Fig. 5 Design artificial layer on Al anode. (a–c) PVDF-coated Al. (a) Schematic illustration of PVDF-Al. (b) Linear polarization curves presenting the corrosion currents for bare Al and PVDF-Al. (c) Comparison of HER initial potentials between PVDF Al and pure Al. Reproduced with permission.[59] Copyright 2022, PERGAMON-ELSEVIER SCIENCE LTD. (d–f) Combination of amorphous Al and polymer coating (Al@a–Al@polymer). (d) Schematic illustration of Al@a–Al@polymer improving the Al stripping/plating reversibility and suppressing HER activity. (e) Comparison of potentiodynamic polarization curves normalized before and after adding amorphous Al layer. (f) Electrochemical stability window (ESW) of aqueous electrolyte (0.5 M $Al_2(SO_4)_3$) obtained by LSV at a rate of 5 mV s^{-1} using Al@a–Al and Al@a–Al-polymer working electrodes, respectively. Reproduced with permission.[60] Copyright 2022, AMER CHEMICAL SOC. (g and h) Combination of $Al_{97}Ce_3$ alloy and MXene coating. (g) Schematic illustration of the fabrication of MXene/E-$Al_{97}Ce_3$ hybrid electrodes. (h) Tafel polarization curves of MXene/E-$Al_{97}Ce_3$, E-$Al_{97}Ce_3$ alloy and monometallic Al electrodes in 2 M Al(OTF)$_3$ aqueous electrolyte at a scan rate of 5 mV s^{-1}. (i) Gas evolution profiles of Al and MXene/E-$Al_{97}Ce_3$ hybrid electrodes during Al stripping/plating progress. Reproduced with permission.[61] Copyright 2023, WILEY-VCH VERLAG GMBH.

negligible hydrogen evolution (Fig. 5i). The symmetric MXene/E-$Al_{97}Ce_3$ cell finally displayed stable stripping/plating voltage profiles over 1000 h.

Obviously, the introduction of artificial interfacial functional layers has an effect on inhibiting gas generation in the operation of ARAMBs, which greatly improves the reliability of ARAMBs. However, due to the diversity and complex composition of artificial interfacial functional layers, it is difficult to investigate the corresponding working mechanism. In addition, although some hydrophobic interfacial layers inhibit the HER activity, they also have negative effects on the charge transfer at the interface,

simultaneously. Therefore, it is important to further unveil the working mechanism and develop more effective functional layers for ARAMBs.

2.3 Aluminium alloy

In addition to building SEI or functional layers on the Al anode, the design of Al alloys by rationally selecting the alloying elements can also shift the standard potential of the anode to a more positive value, thereby enabling the deposition on the metal anode through an underpotential deposition process.[62,63] For example, an oxidation-resistant
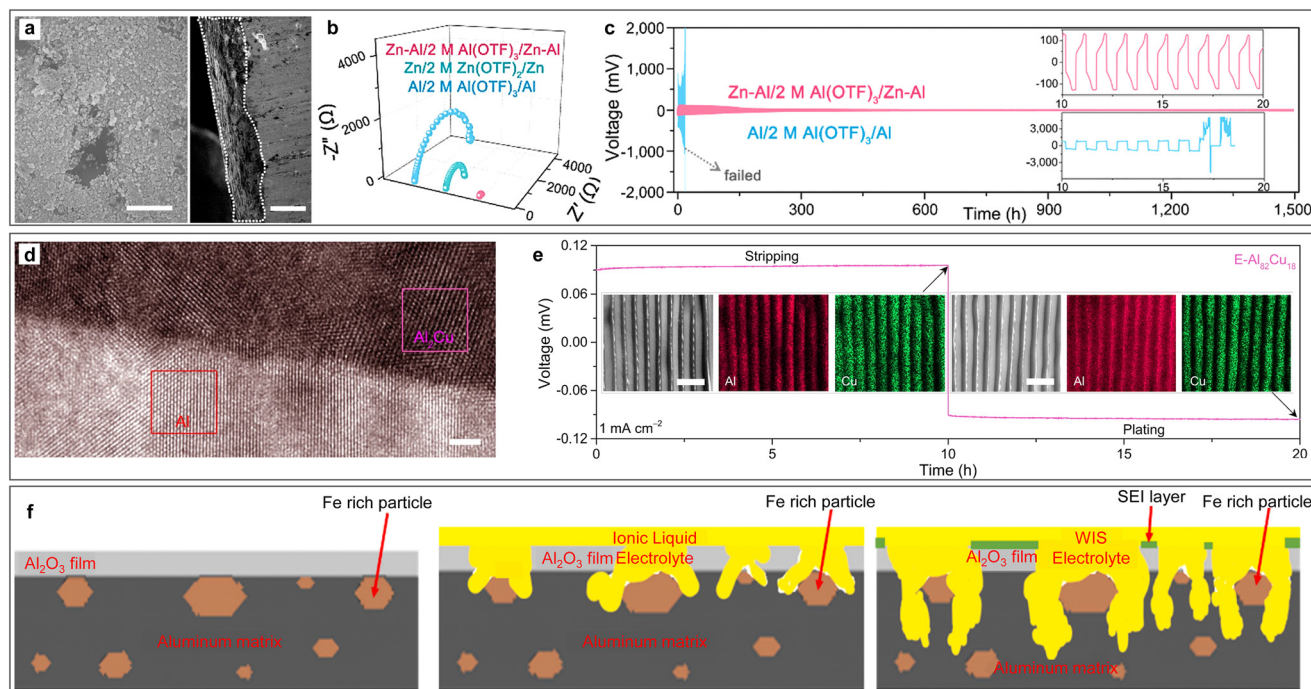
Fig. 6 Aluminium alloy for ARAMBs. (a–c) Zn–Al alloy. (a) SEM images of the top view and cross section of Zn–Al alloy. Scale bars: 500 nm (left) and 30 μm (right). (b) Comparative Nyquist plots of symmetrical cells with different electrodes. (c) Comparison of long-term cycling stability for symmetric cells based on Al and Zn–Al alloy electrodes (0.2 mA cm^{-2}). Reproduced with permission.[64] Copyright 2020, AMER CHEMICAL SOC. (d and e) Eutectic Al$_{82}$Cu$_{18}$ alloy. (d) HRTEM image of Al/Al$_2$Cu interfacial region. Scale bars: 2 nm. (e) Stripping/plating voltage profile of E-Al$_{82}$Cu$_{18}$ symmetric cells at a current density of 1 mA cm^{-2} in 2 M Al(OTF)$_3$ aqueous electrolytes. Insets: SEM images and corresponding EDS mappings of Al and Cu after stripping (left) and plating (right). Scale bars: 1 μm. Reproduced with permission.[66] Copyright 2022, NATURE PORTFOLIO. (f) Schematic illustration of aluminium matrix corrosion during the cycling process in the presence of Al$_3$Fe intermetallic phase. Reproduced with permission.[67] Copyright 2022, ELSEVIER.

and dendrite-suppressed Zn–Al alloy anode was fabricated by depositing Al^{3+} on a Zn substrate (Fig. 6a).[64] The addition of Zn could effectively mitigate the passivation and self-discharge behaviour of the Al anode and improve the CE of the metal stripping/plating process by inhibiting HER. Meanwhile, Zn^{2+} deposits more easily than Al^{3+} because of its higher electrochemical redox potential in aqueous media, and thus the non-deposited Al^{3+} could form a positively charged electrostatic shield to suppress the growth of metal dendrites (Fig. 6b). Given that the co-deposition of Zn^{2+}/Al^{3+} ions effectively reduced the nucleation barrier of Al deposition on the substrate,[47] the Zn–Al alloy anode delivered a small metal stripping/plating voltage polarization for more than 1000 h (Fig. 6c). The battery assembled with the Zn–Al alloy anode and Al$_x$MnO$_2$ cathode delivered a high discharge voltage plateau near 1.6 V and specific capacity of 460 mA h g^{-1} for over 80 cycles. When using tetrachloro-1,4-benzoquinone (TCQ) as the cathode, the cell afforded good cycling stability with 70.7% capacity retention after 200 charge–discharge cycles at a current density of 2 A g^{-1}.[65] In another work, Ran et al. reported the fabrication of a eutectic Al$_{82}$Cu$_{18}$ alloy (E-Al$_{82}$Cu$_{18}$) anode with a lamellar nanostructure consisting of alternating α-Al and intermetallic Al$_2$Cu nanolamellas.[66] The high-resolution transmission electron microscopy (HRTEM) image with

element mapping confirmed the phase separation triggered by the eutectic reaction and the periodic distribution of Al and Cu atoms in the alloy anode (Fig. 6d and e), respectively. When using E-Al$_{82}$Cu$_{18}$ as the anode, the less-noble α-Al lamellas worked as electroactive materials to supply Al^{3+} charge carriers, while the more-noble Al$_2$Cu lamellas served as 2D nanopatterns to guide highly reversible Al stripping and plating at low overpotentials (Fig. 6e), which together endowed the electrodes with exceptional Al stripping/plating stability for more than 2000 h.

Alloying elements can also be introduced through the impurities in Al metal. For example, trace iron impurities in the aluminium metal due to industrial production resulted in the precipitation of the Al$_3$Fe intermetallic phase.[67] Through SEM, it could be observed that the corrosion of the Al matrix preferentially began at the high iron content area and spread between the iron-containing intermetallic phases. The presence of Al$_3$Fe served as a preferential site for the "water-in-salt" (WiS) electrolyte to initiate corrosion of the Al matrix, which promoted the electrolyte to break the passivation oxide barrier to access the Al bulk, and thus accelerated the electrochemical process (Fig. 6f). The above-mentioned report indicates that Al anode treatment with metallurgical techniques is crucial for the development of ARAMBs.

© 2025 The Author(s). Co-published by the Institute of Process Engineering, Chinese Academy of Sciences and the Royal Society of Chemistry

Ind. Chem. Mater., 2025, 3, 7–30 | 13

In conclusion, the use of aluminium alloy anodes has the merits of reducing the voltage hysteresis phenomenon in the galvanostatic test of symmetric batteries, and therefore greatly extends the cycle life of batteries. However, the use of alloy anodes usually sacrifices the discharge potential of the full cell, and thus results in a decrease in energy density. Therefore, the amount and species of alloy metal should be carefully selected.

Therefore, by designing the SEI, artificial interfacial functional layer and aluminium alloy anode, the kinetics of Al stripping process can be largely accelerated with a low overpotential in symmetric Al electrochemical cells (Table 1). However, most strategies are still not sufficiently durable given that the overpotentials inevitably increase during long cycling. Therefore, more approaches need to be developed to prolong the life of ARAMBs.

3 Modification of aqueous electrolytes

Aqueous electrolytes are considered suitable to realize large-scale commercial applications because of their intrinsic advantages such as high ionic conductivity, environmental friendliness, easy accessibility and low cost. As an indispensable constituent of rechargeable aluminium batteries, the electrolyte not only acts as the "ionic bridge" transporting Al^{3+} ions to link the cathode with the anode, but also plays crucial roles in suppressing the HER at the interface and maintaining the reactivity of the Al anode, both of which severely hinder the development and application of ARAMBs. In this section, we summarize the three main current electrolyte modification strategies for ARAMBs including highly concentrated single-salt electrolyte, highly concentrated bi-salt electrolyte, and electrolyte with additive modification. These strategies are usually combined to achieve the optimal electrochemical performance.

3.1 Highly concentrated single-salt electrolyte

The concentration of aqueous electrolytes has a decisive influence on the solvation structures, which have a great impact on the ESW, ionic conductivity and electrolyte/ electrode interface. In the conventional salt concentration, the low reduction voltage of aluminium leads to the inevitable HER. In addition, the passivation film of the aluminium metal anode will rapidly be rebuilt after contacting water. With an increase in the electrolyte concentration, most water molecules will coordinate with metallic cations, and the proportion of free H_2O in the electrolyte gradually decreases. Consequently, the water activity is suppressed and the ESW of the electrolyte is expanded, which will be favourable for the reversible stripping/deposition of Al^{3+} on the aluminium anode.

As a commonly used electrolyte salt in ARAMBs, aluminium trifluoromethanesulfonate ($Al(OTF)_3$) was used to prepare highly concentrated "water-in-salt" electrolytes in 2019.[68] The overall stable window for 5 M $Al(OTF)_3$ aqueous electrolyte is in the range of −0.3 to 3.3 V (*vs.* Al/Al^{3+}). Based on the WiS-$Al(OTF)_3$ electrolyte, the $Al_xMnO_2 \cdot nH_2O$ cathode delivered a specific capacity of 467 mA h g^{-1} and energy density of 481 W h kg^{-1}. In addition to transition metal oxides, the WiS strategy is also used for PBA cathodes. Zhou *et al.* demonstrated a high-capacity PBA-type $FeFe(CN)_6$ cathode with double transition metal redox sites in a similar WiS-$Al(OTF)_3$ electrolyte.[69] The LSV result showed that the WiS-$Al(OTF)_3$ electrolyte exhibited an electrochemical window of 2.65 V (Fig. 7a, cathodic side: 1.65 V *vs.* Ag/AgCl and anodic side: −1 V *vs.* Ag/AgCl). The Tafel plot of H_2 evolution also showed that the overpotential of H_2 in WiS-$Al(OTF)_3$ electrolyte was higher than that in other electrolytes (Fig. 7b), which also confirmed the suppressed reactivity of water in the WiS-$Al(OTF)_3$ electrolyte. The authors further noted that the water molecules in the WiS-$Al(OTF)_3$ electrolyte were not sufficient for the formation of two hydrate shells with Al^{3+}, and thus the electrolyte was dominated by loose ion pairs (LIP) and intimate ion pairs. The fitting result of the Raman spectra showed that the free anion fraction decreased to zero after the concentration of the electrolyte increased to 5 M, while the LIP fraction also increased correspondingly. Therefore, it was concluded that water activity was suppressed due to the strong cation–anion and cation–water interaction in the WiS-$Al(OTF)_3$ electrolyte. Similarly, a potassium nickel hexacyanoferrate cathode also demonstrated stable cycling

Table 1 Cyclic performance of symmetric batteries using different anode modification strategies

Electrode	Electrolyte	Current density (mA cm^{-2})	Overpotential[a] (V)	Cycling life (h)	Ref.
Al treated with $AlCl_3$-[EMIm]Cl IL	2 M $Al(OTF)_3$	0.2	*ca.* 0.2	50	48
Al treated with $AlCl_3$-Acm DES	2 M $Al(OTF)_3$	0.05	0.2	300	56
Al treated with $AlCl_3$-urea ES	2 M $Al(OTF)_3$	0.1	<2	60	58
PVDF-Al	1 M $Al(OTF)_3$	0.1	0.5	100	59
Al@a–Al	0.5 M $Al_2(SO_4)_3$	0.05	0.3	800	60
MXene/E-$Al_{97}Ce_3$	2 M $Al(OTF)_3$	0.5	0.05	1000	61
Zn–Al	2 M $Al(OTF)_3$	0.2	0.025	1000	64
E-$Al_{82}Cu_{18}$	2 M $Al(OTF)_3$	0.5	0.053	2000	66

[a] Overpotential refers to the difference between the potential of symmetrical batteries during charging and discharging at the current density of the same row.
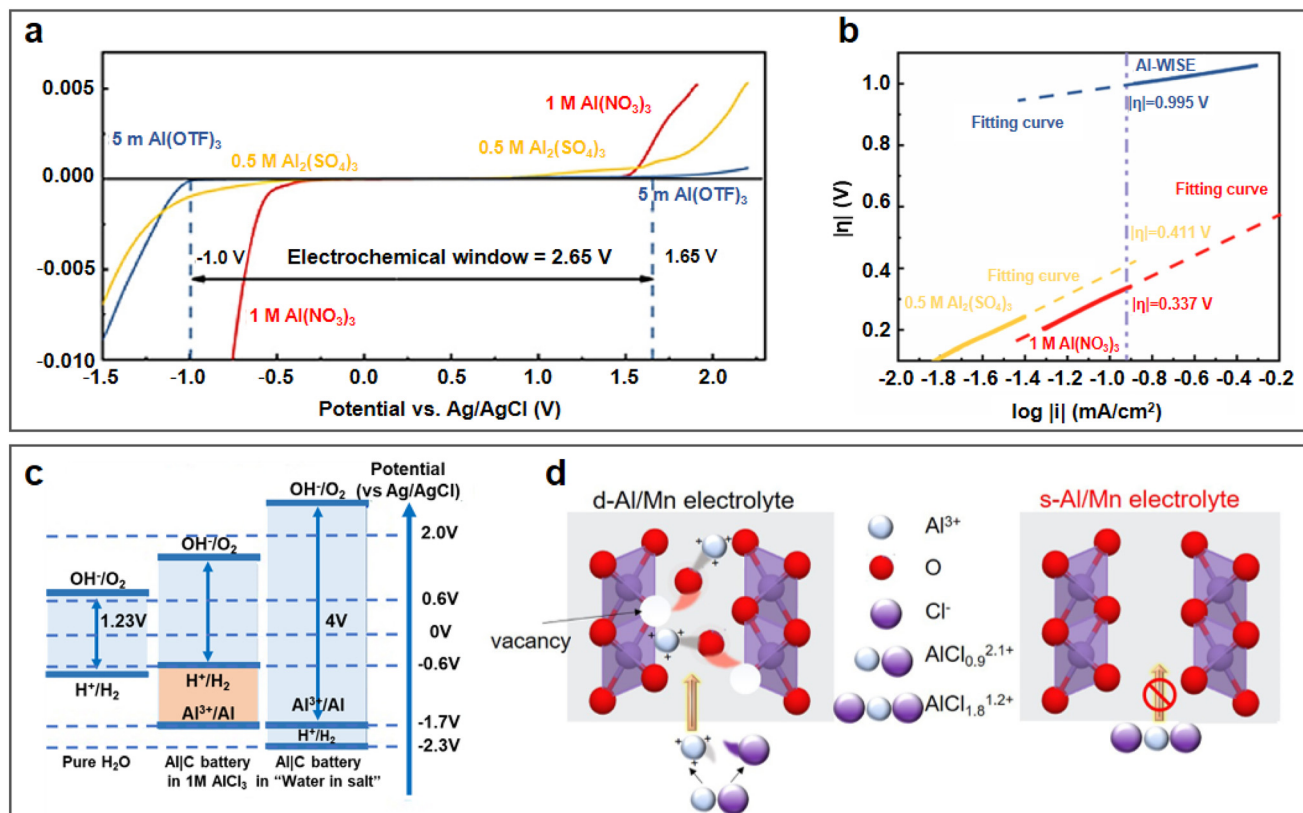
Fig. 7 Highly concentrated single-salt electrolyte. (a and b) WiS-Al(OTF)$_3$ electrolyte. (a) Linear sweep voltammetry of aqueous electrolytes on titanium mesh in a three-electrode system at 10 mV s^{-1} using electrolytes of 5 M Al(OTF)$_3$, 1 M Al(NO$_3$)$_3$, and 0.5 M Al$_2$(SO$_4$)$_3$, respectively. (b) Tafel plot of H$_2$ evolution in different electrolytes. Reproduced with permission.[69] Copyright 2019, AMER CHEMICAL SOC. (c and d) WiS-AlCl$_3$ aqueous electrolytes. (c) Schematic illustration of an expanded ESW for WiS-AlCl$_3$ electrolyte. Reproduced with permission.[71] Copyright 2019, the ROYAL SOCIETY OF CHEMISTRY. (d) Schematic illustration of highly-concentrated electrolyte inhibiting electrochemical dissolution of MnO$_2$. Reproduced with permission.[72] Copyright 2022, ELSEVIER.

up to 500 cycles and maintained its 3D framework structure in the WiS-Al(OTF)$_3$ electrolyte.[70]

In addition to Al(OTF)$_3$, AlCl$_3$ also exhibits excellent solubility in aqueous solution, and thus has been used for the preparation of highly concentrated electrolytes. A WiS-AlCl$_3$ electrolyte (mass ratio of AlCl$_3$·6H$_2$O to H$_2$O was 12) with an ESW of greater than 4 V was used in an Al/graphite full battery.[71] The CV tests showed that the HER voltage in the WiS-AlCl$_3$ electrolyte shifted to less than −2.3 V compared to −0.6 V in the 1 M AlCl$_3$ solution (vs. Ag/AgCl) (Fig. 7c). The lower HER voltage in the WiS-AlCl$_3$ electrolyte allowed Al^{3+} ions to be reduced and deposited on the aluminium anode at about −1.7 V (vs. Ag/AgCl), which was not possible in the dilute solution. Due to the reversible stripping/deposition of the Al anode in the WiS-AlCl$_3$ electrolyte, the Al/graphite full battery achieved a stable life of more than 1000 charge/discharge cycles with a high capacity retention of 99%, even at high current densities (500 mA g^{-1}). When matching with the α-MnO$_2$ cathode, a high discharge voltage of 1.9 V combined with a high discharge capacity of 285 mA h g^{-1} could be achieved, contributing to a high discharge energy density of 370 W h kg^{-1} (based on the mass of MnO$_2$).[73] The WiS-AlCl$_3$ electrolyte not only contributed to the reversible

stripping/deposition behaviour of the Al anode but also the cycling stability of the cathode. The solvation structure of the Al^{3+} cations in the saturated electrolyte (composed of 4.4 M AlCl$_3$ and 1 M MnCl$_2$ in H$_2$O) was larger than in the dilute electrolyte (composed of 1 M AlCl$_3$ and 1 M MnCl$_2$ in H$_2$O), as shown in Fig. 7d, which avoided the intercalation of solvated cations with larger volumes into the MnO$_2$ cathode, and thereby facilitated the stability of the Al/MnO$_2$ battery.[72]

3.2 Highly concentrated bi-salt electrolyte

As mentioned above, by increasing the concentration of the electrolyte, the interaction between cations and water molecules is enhanced, thus reducing the activity of water. In this case, to obtain a higher concentration of electrolyte with a lower content of free water molecules, researchers have developed highly concentrated bi-salt electrolytes, which have been applied in the field of ARAMBs.[74]

A water in bi-salt electrolyte containing supporting Li-salt at a high concentration (1 M Al(OTF)$_3$ + 15 M LiOTF) with a greatly enlarged electrochemical window of up to 4.35 V was reported in 2021.[75] Using an Al$_x$MnO$_2$ cathode, the bi-salt electrolyte enabled a discharge capacity of 160 mA h g^{-1} after

© 2025 The Author(s). Co-published by the Institute of Process Engineering, Chinese Academy of Sciences and the Royal Society of Chemistry
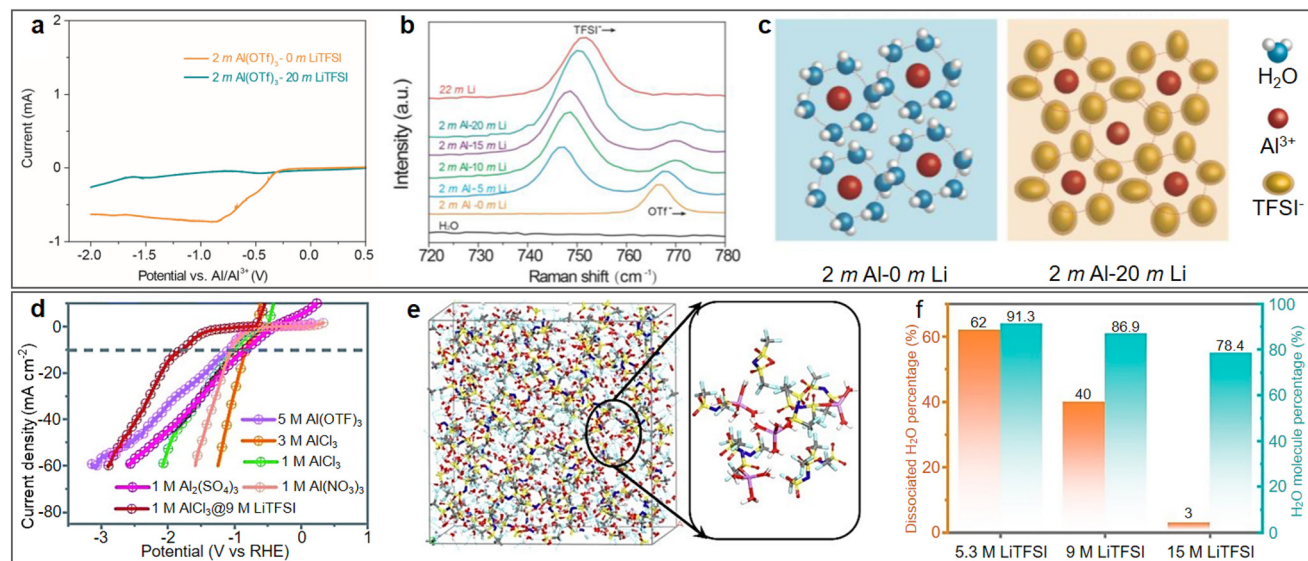
Ind. Chem. Mater., 2025, **3**, 7–30 | **15**

Fig. 8 Highly concentrated bi-salt electrolyte. (a–c) 2 M Al(OTF)$_3$ + 20 M LiOTF electrolyte. (a) Linear sweep voltammetry of Al/Mo cells with different electrolytes. (b) Raman spectra of the electrolytes with varying LiTFSI concentrations. (c) Schematic diagram of solvation structures in bi-salt electrolyte. Reproduced with permission.[76] Copyright 2023, KEAI PUBLISHING LTD. (d–f) AlCl$_3$ + LiTFSI electrolyte. (d) Comparison of different electrolytes in suppressing HER activity. (e) Snapshot of local structure in 0.5 M AlCl$_3$ + 15 M LiTFSI electrolyte. (f) Proportion of dissociated H$_2$O and total H$_2$O in electrolytes containing different concentrations of LiTFSI. Reproduced with permission.[78] Copyright 2022, the ROYAL SOCIETY OF CHEMISTRY.

150 cycles with CE of *ca.* 95%. Similarly, a dual-salt electrolyte with 5 M Al(OTF)$_3$ and 0.5 M LiOTF was proposed with MnO as the cathode.[74] By changing the supporting Li-salt to lithium bis(trifluoromethane sulfonyl) imide (LiTFSI), the resulting bi-salt electrolyte consisting of 2 M Al(OTF)$_3$ and 20 M LiTFSI exhibited an outstanding electrochemical window of close to 3 V.[76] The linear sweep voltammetry of the Al/Mo cells clearly demonstrated the effect of LiTFSI on the electrochemical stability of the aqueous electrolyte (Fig. 8a). With an increase in LiTFSI concentration, the blue shift of the peak at 765 cm^{-1} in the Raman spectra indicated the formation of a considerable amount of contact ion pairs (Fig. 8b). In general, ultra-high concentrations of LiTFSI resulted in a reduction in free H$_2$O around Al^{3+} (Fig. 8c), thus achieving an inhibitory effect on HER. In addition to Li salts, supporting Ca-salts, such as Ca(OTF)$_2$, could also be added to the Al(OTF)$_3$ aqueous solution to broaden its electrochemical window.[77] AlCl$_3$ has also been employed to develop high-performance bi-salt electrolytes. Li *et al.* proposed a series of AlCl$_3$/ LiTFSI aqueous electrolytes with different molar ratios and evaluated their electrochemical performance.[78] The LSV curves (Fig. 8d) suggested that the HER activity in the bi-salt electrolyte with 1 M AlCl$_3$ and 9 M LiTFSI is lower than that in aqueous solutions of other common aluminium salts. The solvation structures in the electrolyte were further investigated by molecular dynamic simulations (Fig. 8e). A portion of water molecules participated in the primary solvation sheath of cations, while others interacted with each other *via* hydrogen bonds. The increase in LiTFSI concentration led to an increase in the proportion of water

molecules involved in the cationic solvation structures. When the concentration of LiTFSI in the electrolyte increased to 15 M, about 97% of the water molecules coordinated with cations (Fig. 8f). The significantly reduced amount of free water molecules helped to suppress the activity of HER reaction, thereby effectively improving the overall performance of the batteries.

3.3 Electrolyte additives

To achieve the optimal electrochemical performance, some electrolyte additives have been added to regulate the chemical environment (for example, pH) in combination with the high-concentration strategy.[79] In aqueous Al/S batteries, it has been reported that the formation of a passivation layer on the Al anode surface could be effectively prevented by adding 0.02 M HCl as an additive to the bi-salt electrolyte (1 M Al(OTF)$_3$ + 17 M LiTFSI).[80] Similarly, the addition of 1 M H$_3$PO$_4$ to the WiS-Al(OTF)$_3$ electrolyte effectively induced the Al^{3+} ions to be bonded to both H$_2$PO$_4^-$ and OTF$^-$ to form complex cations, Al(H$_2$-PO$_4^-$)$_x$(OTF$^-$)$_y$ + (H$_2$O)$_n$, which could mitigate the strong charge densities of the trivalent Al^{3+} and hinder the formation of a passivating film.[81] In addition to changing the chemical environment, some electrolyte additives of soluble low-valence salts of the corresponding cathode metal have been added to inhibit the dissolution of the cathode in the electrolyte. For example, the addition of 0.1 M of Mn(OTF)$_2$ to 2 M Al(OTF)$_3$ electrolyte could effectively increase the discharge capacity and cycle life of TAl/MnO$_2$

full cells, thus achieving more than 100 reversible cycles at a current density of 200 mA g^{-1}.[48]

In summary, increasing the concentration of solutes in aqueous electrolytes plays a significant role in broadening their electrochemical window by regulating the solvation structure of Al^{3+} ions. However, the high salt concentration also increases the overall cost of the battery, and fluorinated salts such as Al(OTF)$_3$ and LiOTF also increase the environmental concerns for subsequent recycling and treatment. In addition, the reported studies on ARAMBs rarely demonstrated the CE of the aluminium metal stripping/deposition behaviour, which is a key challenge for the further development and practical application. Therefore, it may be more feasible to further develop other aqueous electrolyte modification strategies, such as introducing more functional additives or constructing aqueous/organic mixed solvents,[82–84] to achieve highly reversible electrochemical stripping/ deposition behaviour in the aluminium metal by regulating the hydrogen bonding and Al^{3+} ion solvation structure of the electrolyte at lower electrolyte concentrations. Moreover, due to the intricate interfacial issue associated with the Al anode, a synergistic effect between the modification of the anode and electrolyte is usually required to suppress the HER process and facilitate the Al stripping process, simultaneously.

4 Design of cathode materials

ARAMBs are known as promising energy storage devices with a high energy and power density, owing to their three-electron electrochemical mechanism and the small ionic radius of Al^{3+}. However, in practical applications, the high charge density and large hydrated ionic radius of Al^{3+} induce sluggish diffusion dynamics and large electrostatic forces between the host framework and Al^{3+}, leading to the collapse of the cathode materials. Therefore, most cathodes of ARAMBs encounter the challenge of poor cycle stability and slow kinetics. In general, the current research on the cathodes of ARAMBs is still in its infancy, which mainly include vanadium-based materials, manganese-oxide materials, molybdenum-based materials, PBAs, carbon materials and organic materials.

4.1 Vanadium-based materials

Considering their merits of abundant valence states, vanadium-based materials are routinely selected for the fabrication of aqueous batteries, exhibiting a high specific capacity. In recent years, a variety of vanadium-based materials have been studied as cathodes of ARAMBs, including V$_2$O$_5$, VO$_2$-B, VOPO$_4$, FeVO$_4$, KVO, and NH$_4$V$_4$-O$_{10}$.[49,55,78,85–89] In 2019, the electrochemical performance and charge storage mechanism of an orthorhombic V$_2$O$_5$ cathode
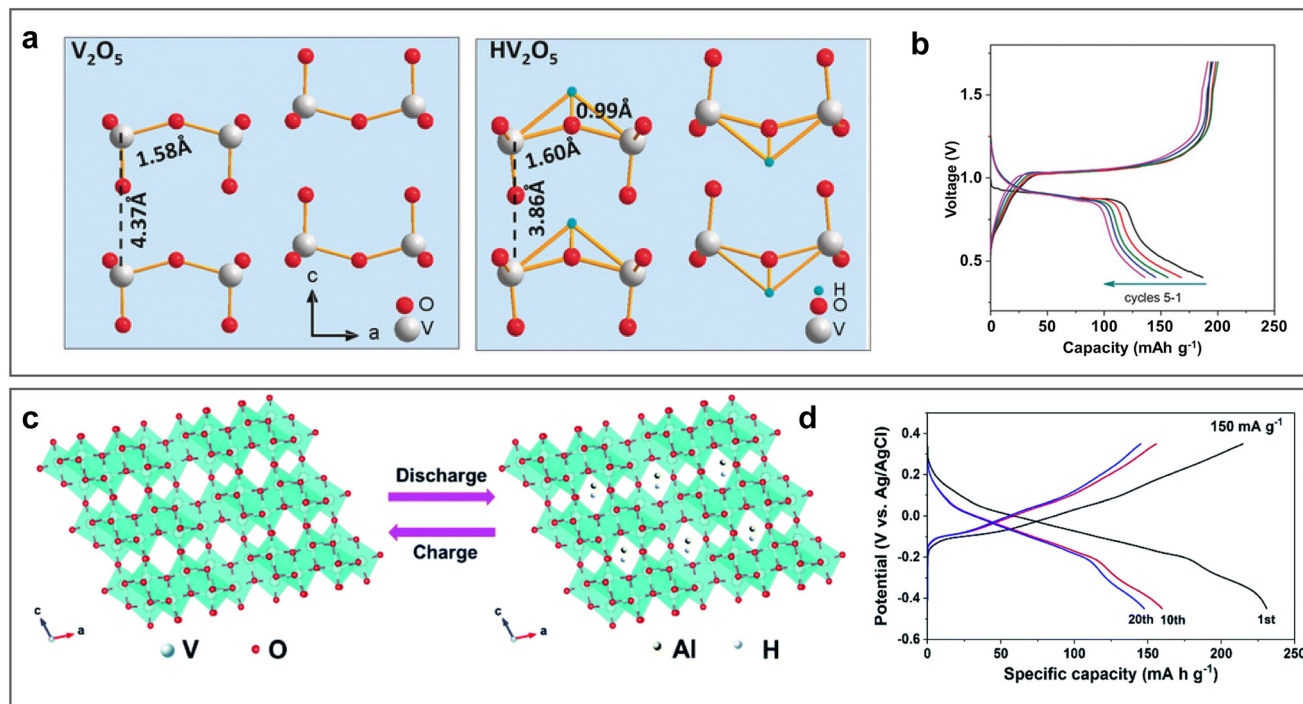

Fig. 9 Vanadium-oxide cathode materials. (a and b) Orthorhombic V$_2$O$_5$. (a) Structure of pristine V$_2$O$_5$ before (left) and after (right) proton intercalation. (b) Galvanostatic charge/discharge (GCD) curves of Al/V$_2$O$_5$ ARAMBs at 40 mA g^{-1} with electrolyte of 2 M Al(OTF)$_3$. Reproduced with permission.[49] Copyright 2020, WILEY-VCH VERLAG GMBH. (c and d) Bronze-type vanadium dioxide (VO$_2$-B). (c) Schematic diagram of H$^+$ and Al^{3+} intercalation/de-intercalation in VO$_2$-B during the discharging and charging processes. (d) GCD curves of Al/VO$_2$-B ARAMBs at 150 mA g^{-1} with electrolyte of 5 M Al(OTF)$_3$. Reproduced with permission.[85] Copyright 2020, the ROYAL SOCIETY OF CHEMISTRY.

© 2025 The Author(s). Co-published by the Institute of Process Engineering, Chinese Academy of Sciences and the Royal Society of Chemistry

Ind. Chem. Mater., 2025, **3**, 7–30 | **17**

were first studied by Zhao *et al.* through experimental and theoretical analysis.[49] In acidic 2 M Al(OTF)$_3$ electrolyte (pH ≈ 2), V$_2$O$_5$ undergoes reversible protonation rather than Al-ion intercalation reaction, providing a specific capacity of 186 mA h g^{-1} (Fig. 9a and b). DFT calculation revealed the stable structure evolution after one proton uptake. Furthermore, the authors found that the intercalation/de-intercalation chemistry depends on the ion concentration and charge density of ions in the electrolyte. Bronze-type vanadium dioxide (VO$_2$-B) with a 2D holey nanobelt morphology was also designed as a cathode of AABs.[85] The large 4.984 Å × 3.281 Å tunnel allowed reversible intercalation/de-intercalation of both Al^{3+} and H$^+$ (Fig. 9c), enabling a high capacity of 234 mA h g^{-1} at 150 mA g^{-1} (Fig. 9d) and a capacity retention of 77.2% after 1000 cycles at 1 A g^{-1}. It is worth mentioning that the electrochemical performance was characterized in a three-electrode system with a high concentration of Al(OTF)$_3$ (5 M). The robust bilayer shear structure and holey nanobelt morphology could not only relieve the lattice stress and volume variation in the discharge/charge cycles but also facilitate the electrolyte/

electrode contact with shortened ion diffusion paths. In addition to intercalation-type cathodes, conversion-type V-based cathodes materials have also attracted interest from researchers. For example, the FeVO$_4$ cathode reacts with Al^{3+} through a transformation from FeVO$_4$ phase to spinel Al$_x$V$_y$O$_4$ and amorphous Fe–O–Al phase, delivering an initial capacity of 350 mA h g^{-1} in the three-electrode system with 1 M AlCl$_3$ electrolyte.[86] However, the capacity rapidly decayed with cycling, which is attributed to the surface reaction between the electrolyte and FeVO$_4$. The formed V$_2$O$_5$ is soluble in acidic electrolyte. In summary, the low operation voltage, sluggish kinetics and poor cycling stability of V-based cathodes are their major issues in AABs. Simultaneously, their cycling performance and reaction mechanism are usually affected by the pH of the electrolyte.

4.2 Manganese-oxide materials

Generally, manganese-oxide cathode materials have the advantages of low cost, high specific capacity, and high operational voltage plateau, but encounter issues such as
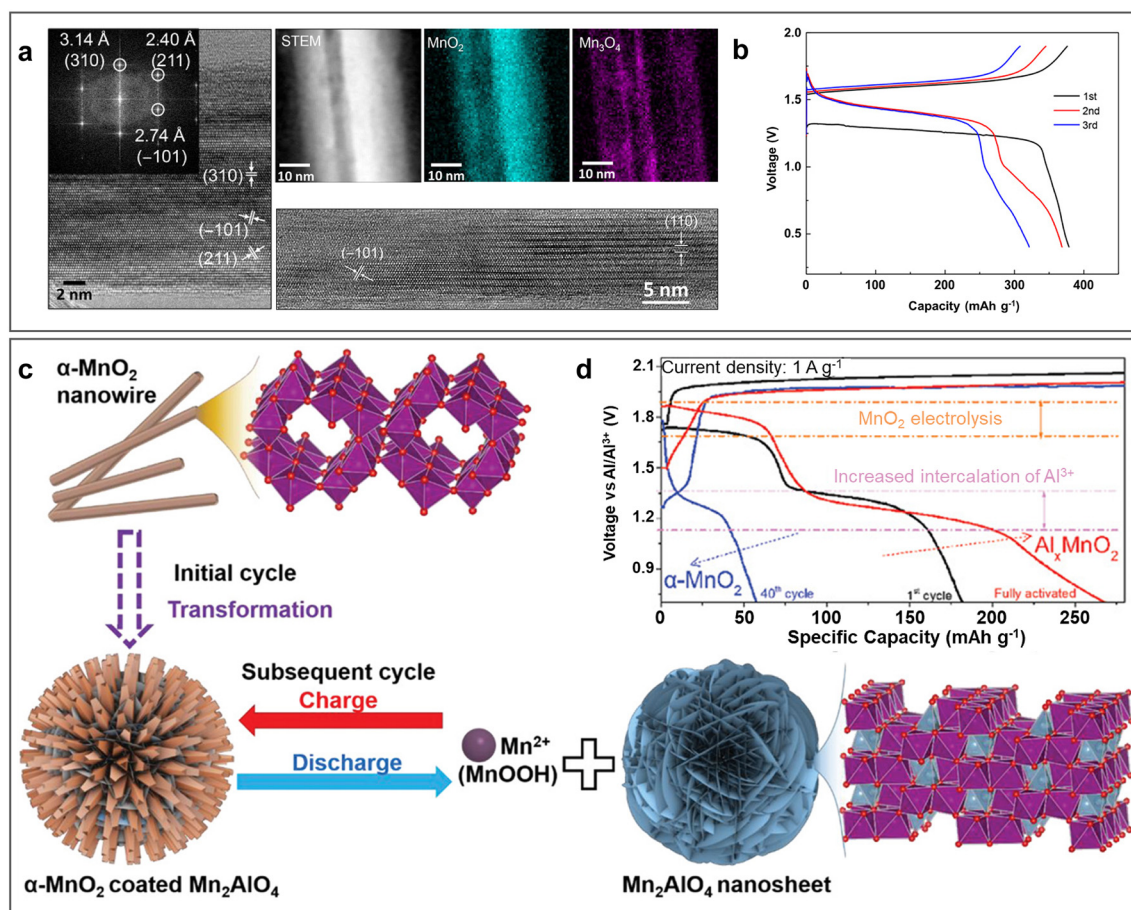

Fig. 10 Manganese-oxide cathode materials. (a and b) α-MnO$_2$ cathode. (a) HRTEM image of α-MnO$_2$ cathode with the fast Fourier transform (FFT) inset (left) before and (right) after discharge with corresponding EELS mapping. (b) GCD curves of Al/α-MnO$_2$ ARAMBs at 100 mA g^{-1} with electrolyte of 2 M Al(OTF)$_3$. Reproduced with permission.[48] Copyright 2018, AMER ASSOC ADVANCEMENT SCIENCE. (c and d) Phase transformation α-MnO$_2$ nanowire cathode. (c) Schematic diagram of transformation from α-MnO$_2$ nanowire to Al$_x$MnO$_2$. (d) GCD curves of Al/α-MnO$_2$ ARAMBs at 1 A g^{-1} with WiS-AlCl$_3$/MnSO$_4$ electrolyte. Reproduced with permission.[73] Copyright 2021, WILEY-VCH VERLAG GMBH.

complicated mechanism and poor stability. In 2018, α-MnO$_2$ nanorods were first reported for ARAMBs in cooperation with an aqueous Al(OTF)$_3$ electrolyte and IL-treated Al anode, displaying a reversible electrochemical discharge/charge process with an initial specific capacity of 380 mA h g^{-1} (Fig. 10b), corresponding to an energy density of about 500 W h kg^{-1} (based on the mass of α-MnO$_2$).[48] The transmission electron microscopy (TEM) images (Fig. 10a) unveiled the formation of a highly crystalline MnO$_2$ core coated by amorphous low-valence Mn oxide shell after discharge. In addition, 0.1 M Mn(OTF)$_2$ was also introduced in the electrolyte to substantially reduce the dissolution of low-valence Mn and improve the cycling stability. Some researchers believed that the pre-addition of Mn^{2+} electrolyte leads to a reversible dissolution/deposition process of the cathode materials. Birnessite MnO$_2$ was found to reduce to Mn^{2+} in the first discharge process in Al(OTF)$_3$ electrolyte with the pre-addition of 0.5 M MnSO$_4$, and then amorphous Al$_x$Mn$_{1-x}$O$_2$ was generated in the following charge process.[90] In the following cycles, it experienced a reversible dissolution/deposition process.

In response to the reaction mechanism, there are some reports suggesting that the mechanisms of the first cycle are different from the following cycles. In the initial cycle, Mn oxides, such as Mn$_3$O$_4$, MnO, and MnO$_2$, are converted to aluminium-containing manganese oxides (Al$_x$MnO$_2$), while Al is not completely extracted in subsequent cycles.[64,68,73] For instance, the spinel Mn$_3$O$_4$ precursor transformed to the mix layered and amorphous phase of Al$_x$MnO$_2$·nH$_2$O during the first charge to 1.8 V in 5 M Al(OTF)$_3$ aqueous electrolyte.[68] The experimental characterization and DFT calculation proved the mechanism that Mn^{2+} in the tetrahedral sites and a part of Mn^{3+} at the octahedral sites dissolved in the electrolyte and the Al^{3+} preferred to insert in the vacant sites due to its low formation energy. It exhibited a specific capacity of 467 mA h g^{-1} mainly from the reversible intercalation/de-intercalation of Al^{3+}. Similarly, the MnO precursor generated Al$_x$MnO$_2$ via topological conversion between rock-salt MnO and MnO$_2$, where Mn^{2+} was partly oxidized to Mn^{4+} and rearranged into the MnO$_2$ phase, while the other Mn^{2+} dissolved.[64] In addition, α-MnO$_2$ nanowires were reported to transform into two phases in the first cycle with the insertion/extraction of Al^{3+} in WiS-AlCl$_3$/MnSO$_4$ electrolyte, which included Mn$_2$AlO$_4$ nanosheets coated by the α-MnO$_2$ nanorods (Fig. 10c).[73] Then, the reversible electrolysis of MnO$_2$ together with the deintercalation of AlCl$_4^-$ and the intercalation of Al^{3+} into Mn$_2$AlO$_4$ contributed to the 1.9 V and 1.2 V discharge plateaus, respectively, in the subsequent cycles. This unique structure enabled a specific of 285 mA h g^{-1} at 500 mA g^{-1} and a high CE of over 95% after 500 cycle at 5 A g^{-1} (Fig. 10d).

To improve the structural stability, a spinel-structured cathode was reported. Al$_{2/3}$Li$_{1/3}$Mn$_2$O$_4$ (ALMO) was synthesized from an LiMn$_2$O$_4$ precursor in 1 M AlCl$_3$/NaCl mixed electrolyte, where Al^{3+} inserted in the lattice and occupied some of the Li$^+$ sites.[91] The diffusion tunnel of the

stable spinel structure provided an excellent rate performance and cycling stability with the reversible intercalation mechanism of Al^{3+}. It exhibited about 145 mA h g^{-1} at the high current density of 1 A g^{-1} with 63% capacity retention after 1000 cycles in Al/AlCl$_3$-NaCl/ALMO cells. The authors noted that the decrease in capacity mainly happened in the initial dozens of cycles due to the dissolution of the cathodes. The defect engineering and cation substitution strategy was also reported to provide an impressive cycle performance in cathodes in the field of ARAMBs. In 2023, Yang *et al.* synthesized cobalt-substituted Mn$_{1-x}$Co$_x$O$_2$ 2D nanosheets and obtained Mn$_{1-x-y}$Co$_x$□$_y$O$_2$ by modulating the defects.[92] According to the experimental and calculation analyses, they revealed that the disorder stacking of nanosheets and porous and crumpled structure enhanced the electrode/electrolyte contact, while the Co-substitution and Mn vacancies significantly improved the electronic conductivity, ion diffusion kinetics of the materials, and effectively inhibited the dissolution of Mn in 2 M Al(OTF)$_3$ aqueous electrolyte. It exhibited a remarkable specific capacity of 585 mA h g^{-1} with an energy density of 685 W h kg^{-1} (based on the mass of the cathode and anode) and high cycling stability (78% over 300 cycles). Overall, the energy density of Mn-based materials is comparatively high among AABs cathodes. Currently, research is focused on inhibiting Mn dissolution and improving the structural stability. In the future, loading carbon materials and synthesizing hydrogel electrolytes may be feasible strategies to further improve the electrochemical performance.

4.3 Molybdenum-based materials

Molybdenum-based materials such as MoO$_3$ exhibit layered structures, which have been investigated as electrode materials due to their characteristic of accommodating various ions with fast kinetics. In 2022, oxygen-deficient MoO$_3$ nanobelts (OD-MoO$_{3-x}$) were prepared *via* the hydrothermal approach and demonstrated the reversible H$^+$ intercalation/de-intercalation mechanism in 1 M AlCl$_3$ electrolyte (pH $\approx$ 2.4).[93] The DFT calculations in combination with experimental characterization indicated the formation of monoclinic H$_{0.6}$MoO$_3$ phase after the first charge process due to the incomplete de-intercalation of H$^+$ in the initial cycle. Therefore, the following cycles experienced the reversible phase transitions of H$_{0.6}$MoO$_3$ $\leftrightarrow$ H$_{1.68}$MoO$_3$ $\leftrightarrow$ H$_2$MoO$_3$ (Fig. 11a). Given that the expansion of the interlayer is caused by the deficiency of oxygen, it achieved an excellent rate capability (97 mA h g^{-1} at the high current density of 50 A g^{-1}, Fig. 11b) with a capacity retention of 67 mA h g^{-1} over 10 000 cycles. The electrochemical storage mechanism of oxygen-deficient MoO$_3$ nanosheets (D-MoO$_3$) was further investigated by Huang *et al.* DFT calculation demonstrated that Al(H$_2$O)$_4$$^{3+}$ was easily absorbed on the (020) surface, while H$_3$O$^+$ inserted into D-MoO$_3$ through the Grotthuss mechanism.[94] Subsequently, H and OH dissociated from H$_3$O$^+$ formed bonds with O and Mo, respectively. In addition

© 2025 The Author(s). Co-published by the Institute of Process Engineering, Chinese Academy of Sciences and the Royal Society of Chemistry

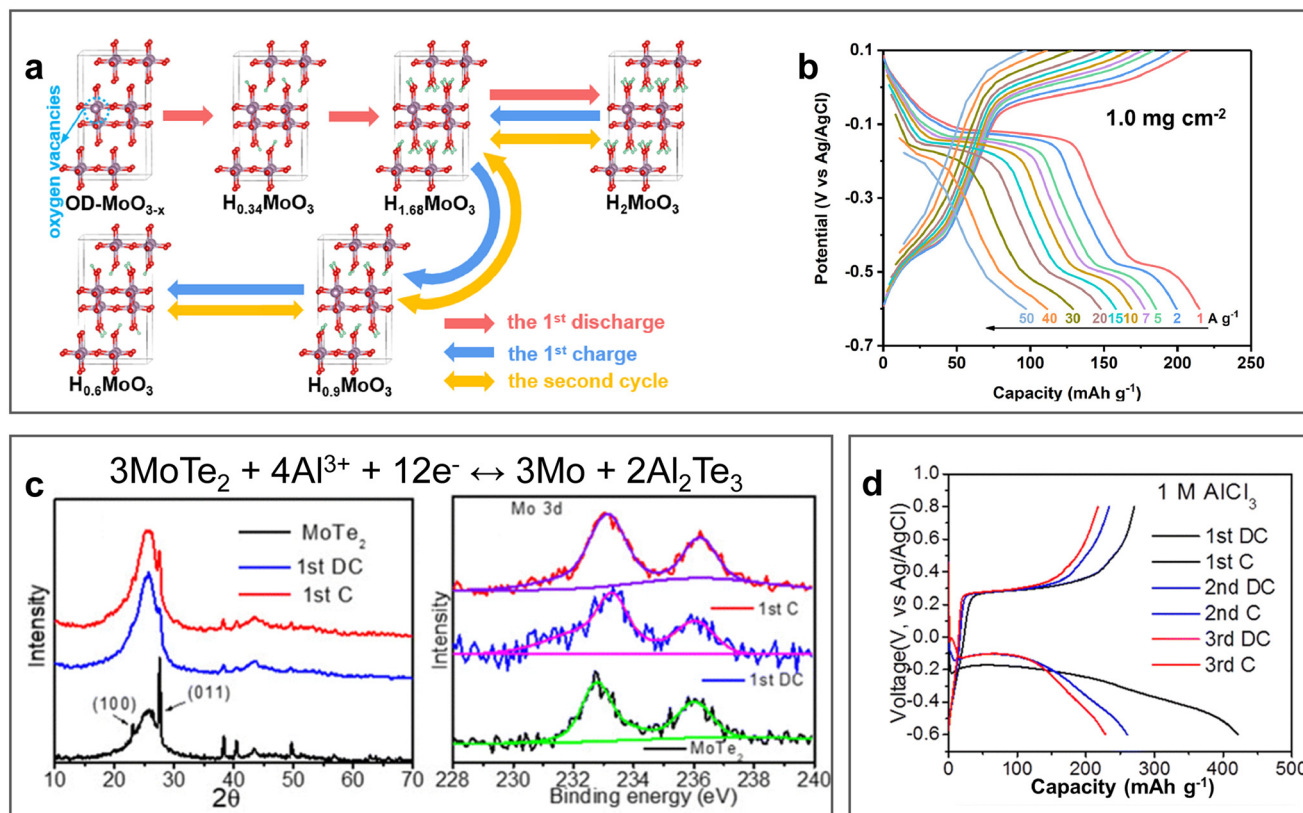*Ind. Chem. Mater.*, 2025, **3**, 7–30 | **19**

Fig. 11 Molybdenum-based cathode materials. (a and b) Oxygen-deficient MoO_3 cathode (OD-MoO_{3-x}). (a) Schematic diagram of H^+ intercalation/de-intercalation mechanism in OD-MoO_{3-x}. (b) GCD curves for OD-MoO_{3-x} cathode in 1 M $AlCl_3$ electrolyte at different current densities. Reproduced with permission.[93] Copyright 2022, ELSEVIER. (c and d) $MoTe_2$ cathode. (c) Electrochemical mechanism, *ex situ* XRD pattern of $MoTe_2$ and *ex situ* XPS spectra of Mo 3d before and after the initial discharge and charge. (d) GCD curves for $MoTe_2$ cathode in 1 M $AlCl_3$ electrolyte at 1 A g^{-1}.[95] Copyright 2023, the ROYAL SOCIETY OF CHEMISTRY.

to MoO_3, two-dimensional molybdenum dichalcogenide layered materials have also been reported, in which hexagonal $MoTe_2$ with an interlayer spacing of 0.69 nm was investigated as an electrochemical storage material for multiple ions.[95] In a three-electrode electrochemical system coupled with 1 M $AlCl_3$ electrolyte, $MoTe_2$ demonstrated the optimal performance with a specific capacity retention of 100 mA h g^{-1} at 1 A g^{-1} over 250 cycles (Fig. 11d). The conversion-type electrochemical mechanism, $3MoTe_2 + 4Al^{3+} + 12e^- \leftrightarrow 3Mo + 2Al_2Te_3$, was illustrated *via* ex situ XRD and XPS analysis of the $MoTe_2$ cathode before and after initial discharge and charge (Fig. 11c). However, a disadvantage of the molybdenum-based electrode materials is their low discharge potential, which limits the energy density of AABs. Nevertheless, they also enable the possibility of constructing an aqueous Al-ion battery with their use as anodes and Mn oxides as cathodes.

4.4 Prussian blue analogues

PBAs are a class of coordination materials with a 3D open framework, which can be generally represented with the chemical formula of $A_xM_1[M_2(CN)_6]_y \cdot nH_2O$, where A represents an alkali metal and M_1 and M_2 represent

transition metals. Their large interstitial sites and diffusion tunnels can facilitate the intercalation/de-intercalation of Al^{3+}.[96] In 2015, Liu *et al.* first applied PBAs as cathodes of AABs (Fig. 12a).[97] In a three-electrode electrochemical system, copper hexacyanoferrate ($KCu[Fe(CN)_6] \cdot 8H_2O$, CuHCF) prepared *via* the co-precipitation strategy exhibited a capacity of 46.9 mA h g^{-1} at 40 mA g^{-1} with a retention of 54.9% over 100 cycles in 0.5 M $Al_2(SO_4)_3$ (Fig. 12b). Since then, several PBA electrodes have been reported for AABs, although most of them were studied in three-electrode electrochemical system. In general, PBAs have the advantages of simple synthesis, low cost, and high rate and cycling performance, whereas their disadvantage of low specific capacity and low discharge voltage still need to be improved.

Vacancy modulation has been reported as an effective method to promote the rate performance and enhance the capacity through the activation of redox sites. Employing this strategy, $Mn_4[Fe(CN)_6]_{2.88}\Delta_{0.29} \cdot 11.8H_2O$ (MnFe-PBA) was prepared *via* the co-precipitation strategy with $Fe(CN)_6$ vacancies, which achieved a high capacity of 106.3 mA h g^{-1} at 0.2 A g^{-1} with the average discharge voltage of 1.2 V (Fig. 12c).[52] Taking advantage of the two reactive metal redox sites of Fe^{3+}/Fe^{2+} and Mn^{3+}/Mn^{2+}, MnFe-PBA showed reversible 1.2 Al^{3+} insertion/extraction with a change in

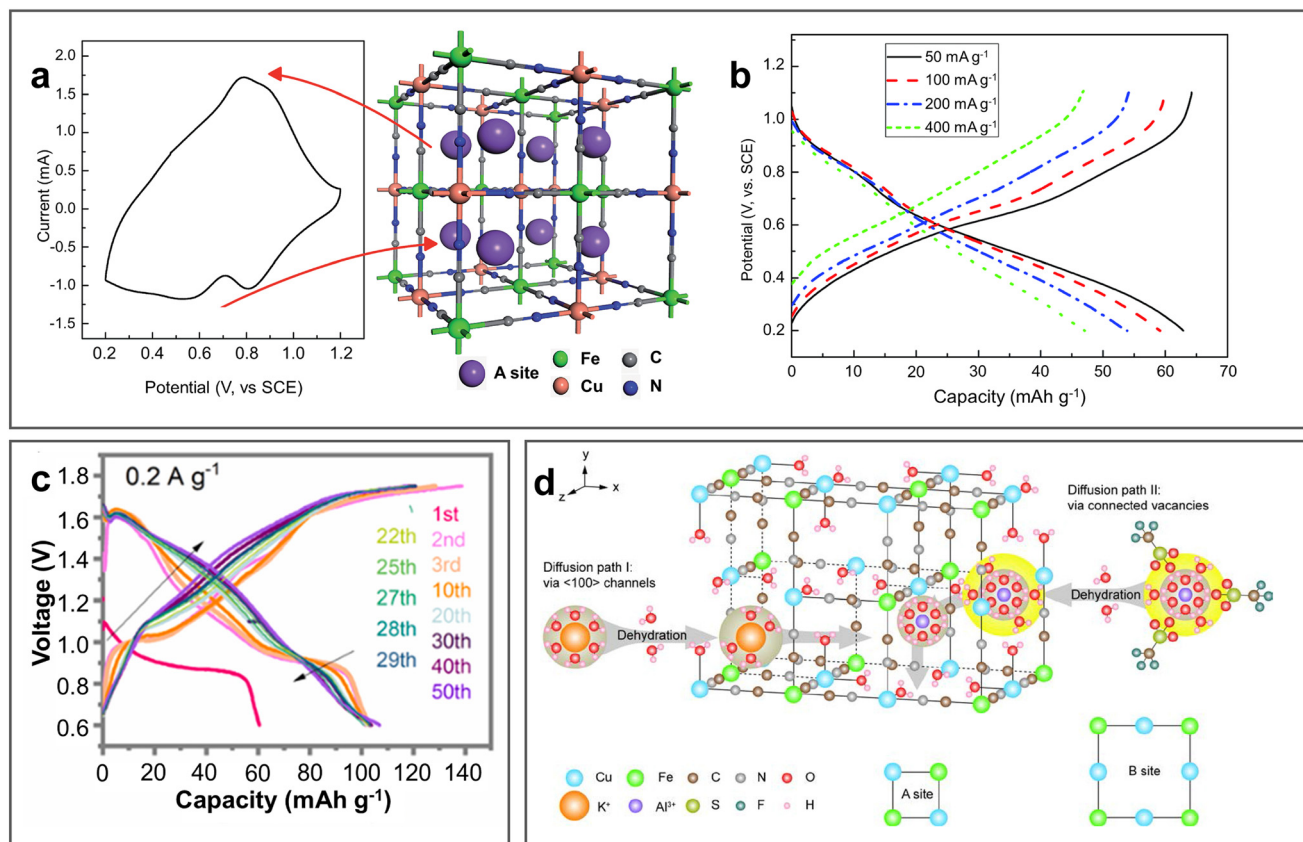**Fig. 12** PBA cathode materials. (a and b) $KCu[Fe(CN)_6]\cdot 8H_2O$ (CuHCF) cathode. (a) CV curve of CuHCF cathode in 0.5 M $Al_2(SO_4)_3$ electrolyte with its crystal structure after Al^{3+} intercalation. (b) GCD curves for CuHCF in same electrolyte at various current densities. Reproduced with permission.[97] Copyright 2015, the ROYAL SOCIETY OF CHEMISTRY. (c) GCD curves for Al/MnFe-PBA ARAMBs at 0.2 A g^{-1} with electrolyte of 1 M Al(OTF)$_3$. Reproduced with permission.[52] Copyright 2021, ELSEVIER. (d) Crystal structure of $K_{0.03}Cu[Fe(CN)_6]_{0.65}\cdot 2.7H_2O$ (CuHCFe) with two possible diffusion channels. Reproduced with permission.[98] Copyright 2023, ELSEVIER SCI LTD.

structure between cube and monocline, and transformed to the tetragonal phase due to the Jahn–Teller effect with an increase in the content of Mn^{3+} after 50 cycles. Also, its cycling life could be further improved to over 200 cycles using a nano-fibrillated cellulose/polyacrylamide (NFC/PAM) gel electrolyte. As shown in Fig. 12d, $K_{0.03}$-$Cu[Fe(CN)_6]_{0.65}\cdot 2.7H_2O$ with two redox sites (Cu^+/Cu^{2+}, Fe^{3+}/Fe^{2+}) can not only provide both the (100) channels of traditional A sites and enlarged ion diffusion paths linked by $Fe(CN)_6$ vacancies, but also shield the coulombic interactions between Al^{3+} and the host lattice by interstitial water.[98] Consequently, it only underwent 2.5% volume change during the charge/discharge process, contributing to the outstanding rate performance (73% capacity at 50 C with average CE of 99.92%) and cycling stability (96% retention at 70 mA g^{-1} for over 3000 cycles) in 1 M Al(OTF)$_3$. By comparing different aluminium salt aqueous solutions and pure acid electrolyte, the authors revealed that the type of anion instead of pH determined the electrochemical performance. Among them, OTF$^-$ exhibited the best performance (Al(OTF)$_3$ > Al(NO$_3$)$_3$ > Al$_2$(SO$_4$)$_3$) on account of the one order of magnitude larger diffusion coefficient of Al^{3+} during the faradaic processes. Morphology design is helpful to improve the electrochemical

performance of PBAs. For example, the $K_2CoFe(CN)_6$ framework with highly stacked structures can decrease the length of ion transport.[99] Self-assembled Fe–Co PBA with a multi-void nano-frame structure exposed plenty of active sites and relieved volumetric changes during cycling.[100] In addition, preintercalation strategy was also investigated, which can effectively expand the ion diffusion channels, improve the ionic conductivity, inhibit structural changes, and enhance the cycling stability. CuHCF achieved the best performance after preintercalation in 0.1 M $Al_2(SO_4)_3\cdot 18H_2O$ solution at 40 °C.[98] It showed 1.6 times higher capacity than the original sample and 80.3% capacity retention over 5000 cycles with a high CE of nearly 100%.

The reaction mechanism and working potential of PBAs can also be affected by the electrolyte concentration. $KCoFe(CN)_6\cdot 5.5H_2O$ (CoHCF) was synthesized via a simple coprecipitation method and its energy storage mechanism was investigated in saturated AlCl$_3$ aqueous electrolyte, achieving a specific capacity of 103.5 mA h g^{-1}.[101] The experimental characterization demonstrated that CoHCF can undergo reversible Al^{3+} and H^+ intercalation/de-intercalation together with the redox reaction of the Cl^-/Cl^0 pair at high potential, which was influenced by both the concentration of

© 2025 The Author(s). Co-published by the Institute of Process Engineering, Chinese Academy of Sciences and the Royal Society of Chemistry

Ind. Chem. Mater., 2025, **3**, 7–30 | **21**

$Al_2Cl_7^-$ and the CoHCF catalyst. With an increase in the concentration of $AlCl_3$, the discharge capacity increased in the high potential platform and reached the maximum when the concentration reached saturation. The reversible Cl^-/Cl^0 redox reaction promoted a high average discharge voltage of 1.65 V and high energy density of 155 W h kg^{-1} (based on the cathode material and Al anode), while the $AlCl_3$ electrolyte enhance the cycling capacity (94.7% over 1200 cycles in Al/CoHCF battery).

In summary, PBAs exhibit outstanding cycling stability due to their large tunnels and small volume changes during the intercalation/de-intercalation of Al^{3+}. However, their specific capacity needs to be improved urgently. Moreover, most of them are currently tested in the three-electrode system. Also, their electrochemical performance needs to be further investigated when matched with metal-Al anodes.

4.5 Carbon materials

Carbon materials, especially graphite-based carbon materials, are widely used as cathodes in aluminium batteries with ionic liquid electrolyte systems due to their remarkable cycling stability with high out-put voltage. In 2019, graphite was used as a cathode by Pan *et al.* in ARAMBs by using WiS-$AlCl_3$ electrolyte.[71] The assembled Al/WiS-$AlCl_3$/graphite batteries displayed a high capacity retention of about 99% over 1000 cycles. Graphite was reported to exhibit a dual-ion intercalation mechanism, including the insertion of Al^{3+} and the extraction of $AlCl_4^-$ during the discharge process, in which the voltage plateau was affected by the concentration of $C_x[AlCl_4]$ in graphite. Furthermore, a one-dimensional

single-walled carbon nanotube (SWCNT) was also applied as a cathode material in WiS-$AlCl_3$ electrolyte.[102] Matching with the Al anode, SWCNT also revealed a multiple ion intercalation mechanism, realizing a capacity of 790 mA h g^{-1} at 5 A g^{-1}, in which the de-intercalation of $AlCl_4^-$ could provide the high discharge voltage plateau of 1.8 V and Cl^- could assist the intercalation of Al^{3+} and H^+ with an extended discharge voltage plateau at 1.2 V (Fig. 13a and b).

In addition, two-dimensional reduced graphene oxide (rGO) synthesized by the freeze-drying method was also reported for ARAMBs with $Al(OTF)_3$ electrolyte.[103] rGO is endowed with a large interlayer spacing, small crystallite size (Fig. 13c and d) and high hydrophobicity, enabling a pseudocapacitive charge storage mechanism with an energy density of 136 W h kg^{-1} (based on the mass of the cathode, Fig. 13e). $[Al(H_2O)_6]^{3+}$, as the main cation in the electrolyte, did not require desolvation during insertion and acted as a proton donor to contact with oxygen in rGO, which promoted the formation of an electrochemical double layer and stabilized the rGO structure effectively. In general, carbon materials with abundant active sites show good cycling stability. However, there are few reports on the use of carbon materials for the fabrication of ARAMBs, and their electrochemical mechanism still need to be further clarified.

4.6 Organic materials

Different from the conventional inorganic materials, where the electrochemical reaction is limited by the inner space in their crystal lattice, organic electrode materials with the merits of diverse designs, adaptable structures, and flexible

Fig. 13 Carbon-based cathode materials. (a and b) Single-walled carbon nanotube cathode (SWCNT). (a) Schematic diagram of multi-ion intercalation/de-intercalation mechanism during charge/discharge process. (b) GCD for Al/SWCNT ARAMBs at various current densities with WiS-$AlCl_3$ electrolyte. Reproduced with permission.[102] Copyright 2021, WILEY-VCH VERLAG GMBH. (c and e) Reduced graphene oxide (rGO) cathode. (c) SEM image and (d) XRD of rGO. (e) GCD for Al/RGO ARAMBs at various current densities with 2 M $Al(OTF)_3$ electrolyte. Reproduced with permission.[103] Copyright 2022, WILEY.

Fig. 14 Organic cathode materials. (a and b) Phenazine (PZ) cathode. (a) Al(OTF)$^{2+}$ storage mechanism in PZ. (b)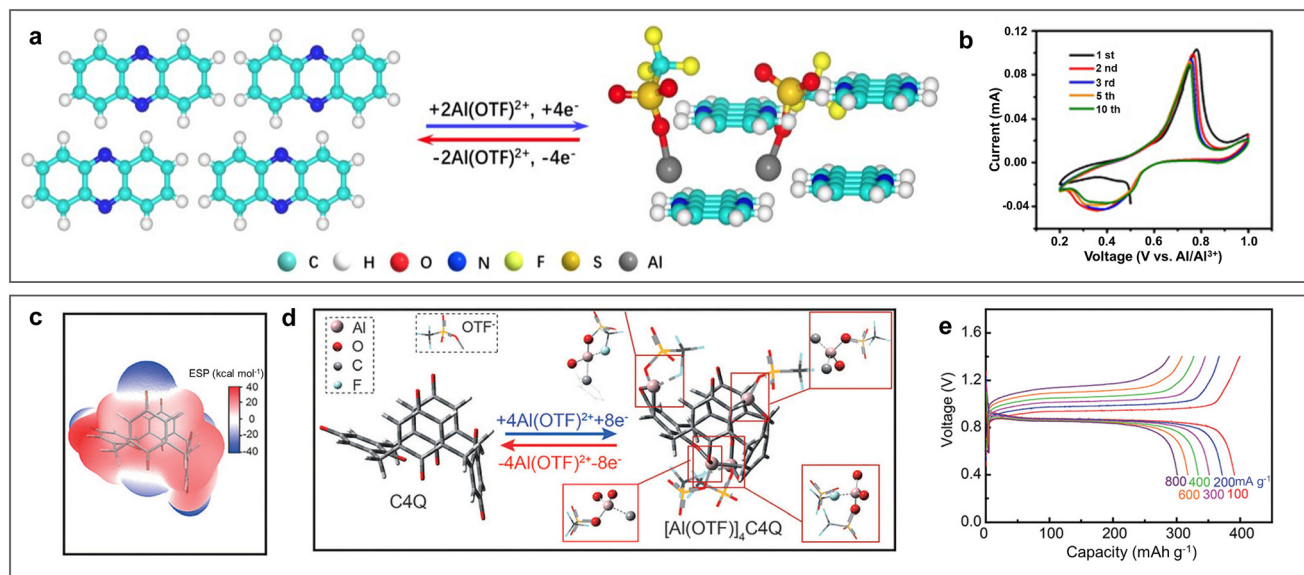 CV curves of Al/PZ ARAMBs at 0.1 mV s^{-1} with electrolyte of 5 M Al(OTF)$_3$. Reproduced with permission.[106] Copyright 2021, WILEY-VCH VERLAG GMBH. (c and e) Calix[4]quinone (C4Q) cathode. (c) ESP and (d) optimized structures of C4Q before and after Al(OTF)$^{2+}$ uptake. (e) GCD curves of Al/C4Q ARAMBs at various current densities with electrolyte of 1 M Al(OTF)$_3$. Reproduced with permission.[53] Copyright 2021, WILEY-VCH VERLAG GMBH.

frameworks have attracting increasing attention.[104,105] In 2020, phenazine (PZ) was first employed as a cathode by Chen *et al.* for ARAMBs in 5 M Al(OTF)$_3$ electrolyte, where a high concentration of OTF$^-$ decreased the solvation effect of H$_2$O.[106] The large conjugated system and flexible structure of PZ facilitated the intercalation/de-intercalation of large-sized ions and improved the structural stability. The C=N redox active centre was found to be reversibly coordinated with Al(OTF)$^{2+}$ rather than Al^{3+}, which could reduce the desolvation energy and coulombic interactions effectively (Fig. 14a and b). Quinone electrodes with carbonyl (C=O) as redox sites have also been investigated as cathodes for ARAMBs. By comparing a variety of quinone electrodes, Li *et al.* found that macrocyclic calix[4]quinone (C4Q) exhibited excellent electrochemical behaviour in terms of energy density, rate capability and low-temperature performance.[53] The large cavity and sterically multi-adjacent carbonyls in C4Q made it easier for intramolecular Al(OTF)$^{2+}$ coordination with small structural change, achieving a high specific capacity of 400 mA h g^{-1}. Impressively, a pouch-type ARAMB was first assembled by using the Al/C4Q battery system, achieving a high energy density of 93 W h kg^{-1} with a low polarization of 42 mV (Fig. 14c–e). Benefiting from the designability of organic electrode materials, tetrachloro-1,4-benzoquinone was designed for ARAMBs.[65] The inductive effect of the Cl$^-$ electron-withdrawing group increased the electrochemical activity of carbonyl, showing a specific capacity of 144 mA h g^{-1} through the reversible enolization of carbonyls.

Polymerization is known as an effective way to inhibit solubility and improve the electronic conductivity of organic cathodes materials. Poly(2,3-diaminophenazine) (PDAP)

electropolymerized on carbon substrates exhibited high electronic conductivity and low solubility due to its long-range conjugated skeleton, as well as strong intermolecular interactions, such as hydrogen boding and π–π interaction collaboration with carbon.[107] Meanwhile, PDAP is a bi-polar organic cathode with n-type (C=N) and p-type (N–H) electroactive groups, demonstrating reversible storage capability for Al^{3+}, H$^+$ and ClO$_4^-$ with long-life stability for over 1000 cycles in Al/1 M Al(ClO$_4$)$_3$/PDAP cells. In addition, the nonconjugated organic electroactive material 2,2,6,6-tetramethylpiperidyl-1-oxy (TEMPO) was also investigated by *in situ* electrochemical characterization.[108] In aqueous electrolyte, hydrolysis, ligand exchange and protonation can generate TEMPOH$_2^+$, which can result in comproportionation with TEMPO$^+$ and allow a reversible electrochemical reaction. Poly(TEMPO methacrylate) (PTMA) provided a capacity of over 110 mA h g^{-1} at 4 C with a CE close to 100% and capacity retention of 77% after 800 cycles. In summary, organic cathodes have the advantage of high specific capacity, with the disadvantages of low conductivity and dissolution. Thus, combining carbon materials and polymerization is a promising strategy to improve the conductivity and resolve the dissolution problems.

In summary, the electrochemical performances of the above-mentioned types of cathodes are listed in Table 2, among which transition metal oxide materials are the most studied, carbon materials achieved the highest specific capacity, and PBAs exhibited the best cycling stability. However, it should be mentioned that the evaluation standards are not uniform, including three-electrode system and Al anodes. The cycle life is usually much higher in the three-electrode system given that the electrochemical

Table 2 Electrochemical performance of ARAMBs with various cathode materials

Cathode	Anode	Electrolyte	Capacity (mA h g^{-1}, mA g^{-1})	Cycling performance [retention, cycles (mA g^{-1})]	Ref.
V_2O_5	TAl	2 M Al(OTF)$_3$	186, 20	65%, 50/20[a]	49
VO_2-B	—	5 M Al(OTF)$_3$	237, 150	77.2%, 1000/1000[b]	55
$FeVO_4$	—	1 M AlCl$_3$	350, 60	10%, 20/60[b]	86
$VOPO_4 \cdot 2H_2O$	Al	2.5 M Al(OTF)$_3$	125.4, 20	60%, 40/20[a]	85
$NH_4V_4O_{10}$	Zn–Al	2 M Al(OTF)$_3$	241.76, 1000	43%, 100/1000[a]	88
KVO	Al	0.5 M AlCl$_3$ + 12 M LiTFSI	223, 1000	64.6%, 300/4000[b]	78
α-MnO$_2$	TAl	2 M Al(OTF)$_3$	380, 100	44%, 40/100[a]	48
Cryptomelane MnO$_2$	—	1 M Al(NO$_3$)$_3$	109, 20	61.6%, 60/20[b]	109
Bir-MnO$_2$	TAl	2 M Al(OTF)$_3$ + 0.5 M Mn(OTF)$_2$	554, 100	57.7%, 65/100[a]	90
Al$_x$MnO$_2 \cdot n$H$_2$O (Mn$_3$O$_4$)	Al	5 M Al(OTF)$_3$	467, 30	58%, 50/30[a]	68
Al$_x$MnO$_2$ (MnO)	Zn–Al	2 M Al(OTF)$_3$ + 0.2 M Mn(OTF)$_2$	460, 100	/[a]	64
Al$_x$MnO$_2$ (α-MnO$_2$)	Al	AlCl$_3 \cdot 6$H$_2$O : MnSO$_4 \cdot 6$H$_2$O : H$_2$O = 4 : 1 : 1 (mass ratio)	285, 1000	95%, 500/5000[c]	73
Al$_{2/3}$Li$_{1/3}$Mn$_2$O$_4$	—	1.0 M AlCl$_3$/NaCl	152, 100	67.4%, 1000/1000[b]	91
	Al		162, 100	89.4%, 230/1000[d]	
Mn$_{1-x-y}$Co$_x$□$_y$O$_2$	Al	2 M Al(OTF)$_3$	585, 100	78%, 300/100[a]	92
BQ-Al$_x$MnO$_2$	Zn–AL	2 M Al(OTF)$_3$ + 0.2 M Mn(OTF)$_2$	300, 1000	90%, 800/1000[a]	110
OD-MoO$_{3-x}$	—	1 M AlCl$_3$	97, 50 000	69.1%, 10 000/50 000[b]	93
D-MoO$_3$	—	0.5 M Al$_2$(SO$_4$)$_3$	167.39, 5000	73.6%, 1000/5000[b]	94
MoTe$_2$	—	1 M AlCl$_3$	420, 1000	23.8%, 250/1000[b]	95
CuHCF	—	0.5 M Al$_2$(SO$_4$)$_3$	63, 50	54.9%, 1000/400[b]	97
KNHCF	Al	5 M Al(OTF)$_3$	46.5, 20	52%, 500/20[a]	70
CuHCF	—	1 M AlCl$_3$	54.5, 1000	80.3%, 5000/1000[b]	111
CuHCFe	—	1 M Al(OTF)$_3$	69.35, 70	70%, 2300/350[b]	98
K$_2$CoFe(CN)$_6$	—	1 M Al(NO$_3$)$_3$	50, 100	76%, 1600/100[b]	112
MnFe-PBA	TAl	1 M Al(OTF)$_3$	106.3, 200	69.5%, 100/500[a]	52
FF-PBA	—	5 M Al(OTF)$_3$	97.62, 150	60.8%, 100/150[b]	69
CoHCF	Al	Saturated AlCl$_3$	103, 50	94.7%, 1200/250[e]	101
Graphite	Al	AlCl$_3 \cdot 6$H$_2$O : H$_2$O = 0.8 : 1 (mass ratio)	165, 500	99%, 1000/500[a]	71
SWCNT	Al	AlCl$_3 \cdot 6$H$_2$O : H$_2$O = 10 : 1 (mass ratio)	790/5000	/[b]	102
rGO	TAl	2 M Al(OTF)$_3$	136, 50	60% 90/50[a]	103
PZ	Al	5 M Al(OTF)$_3$	132, 50	76.5% 300/50[a]	106
C4Q	TAl	1 M Al(OTF)$_3$	400, 40	81%, 50/200[a]	53
TCQ	Zn–Al	1 M Al(OTF)$_3$	147.7, 200	70.7%, 200/2000[a]	65
PDAP	Al	1 M Al(ClO$_4$)$_3$	321, 100	65%, 1000/2000[a]	107
PTME	Al	1 M Al(OTF)$_3$	111, 2 C	77%, 800/4 C[d]	108

[a] Coin cell. [b] Three-electrode system. [c] PMMA cell. [d] Swagelok-type cell. [e] Dual electrolytic cell.

performance is not affected by Al metal anodes. Meanwhile, the mass loading of the cathode is generally low, which needs to be further increased for practical applications.

5 Summary and outlook

In summary, considerable efforts have been devoted to each component of ARAMBs to stabilize their electrochemical performance. To facilitate the Al stripping process and suppress the HER reaction, the intrinsic highly passivated Al surface is removed with the formation of an ionic liquid analogue-derived SEI or artificial layer. In addition, the fabrication of Al alloys can shift the potential of the anode, and thus suppress the HER process. The design of the electrolyte is also crucial to reduce the parasitic reactions and maintain long cycle stability in batteries. Building highly concentrated electrolytes and adding additives that are widely used in other aqueous batteries are also feasible for ARAMBs. Finally, due to the high charge density of the Al^{3+} ion, the cathode materials are mostly vanadium-based materials,

manganese-oxide materials, molybdenum-based materials, PBAs, carbon materials and organic materials. The reaction can be based on the conversion, intercalation or charge compensation mechanism, where Mn-based and organic cathodes generally exhibit a higher specific capacity than other materials. However, although intriguing progress has been made, the development of ARAMBs is still in its infancy and a few issues need more attention in future studies (Fig. 15).

1) Simultaneously meeting the requirements of fast Al stripping kinetics and suppression of the HER process. The dense passivation film with a high band-gap on the Al anode is known to cause sluggish kinetics for Al stripping, thus leading to a low operation voltage in ARAMBs. Also, although the kinetics improves when the passivation film is removed, it also usually accelerates the generation of H$_2$.

2) The reversibility of Al anode under aqueous electrolyte during repeated cycling. The CE of Al stripping/plating in IL-based electrolytes such as AlCl$_3$-[EMIm]Cl has reached over 99%. However, the reversibility in aqueous electrolyte is
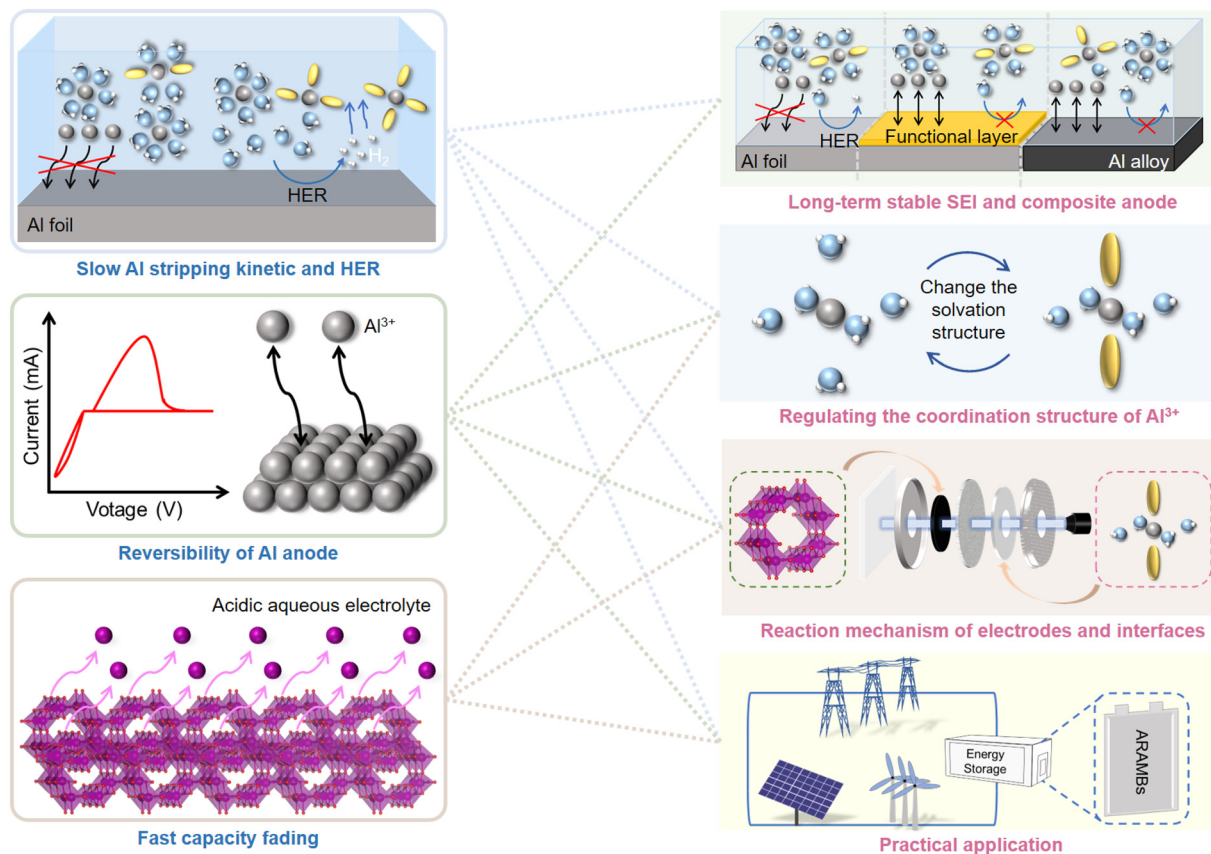
Fig. 15 Summary and outlook of rechargeable aqueous aluminium metal batteries.

inferior and leads to the continuous consumption of Al during cycling.

3) The fast capacity fading on the cathode side in acidic aqueous aluminium electrolyte. Given that most Al salts such as $Al(OTF)_3$, $Al_2(SO_4)_3$, and $AlCl_3$ are known as strong acid and weak base salts, low pH makes the design of cathodes difficult. Most metal oxide cathodes are soluble during the discharge process, leading to low cycling life in batteries. Meanwhile, the high charge density of Al^{3+} leads to large electrostatic interaction with the lattice and high volume change, resulting in a poor kinetic performance and low reversibility.

Due to the ever-growing ratio of renewable energy in electric power generation, its intermittent characteristic accelerates the need for electrochemical energy storage systems. In this case, the emerging ARAMBs are endowed with several merits, including high abundance Al resource, high specific capacity of Al anode, cost efficiency and improved safety of aqueous electrolytes, which are promising candidates in the future smart grid if their electrochemical performance can be further enhanced. We prospect that further studies should be focused on the following aspects.

1) Developing long-term stable SEI and composite anodes. As a metal anode, the repetitive stripping/plating process during the discharge/charge process will lead to the rupture of the interphase, resulting in the formation of a highly

passivated oxide interphase. Accordingly, the construction of an inorganic/polymer interphase may be a possible strategy to resolve this issue, in which inorganic compounds provide decent ionic conductivity to transport Al^{3+} and elastic polymers can accommodate the volume changes during the Al stripping/plating process.

2) Regulating the coordination structure of Al^{3+} in aqueous electrolytes. It is known that coordinated H_2O is easily transferred to the anode side in the presence of an electric field and inducing the HER process. In this case, the introducing of an organic component in the electrolyte that is prone to coordination with Al^{3+} seems to be a possible approach to suppress the HER reaction. When the organic component moves to the anode side with Al^{3+}, its reduction will generate a new interphase rather than H_2. In addition, the coordination structure of Al^{3+} has a significant influence on the reversibility of electrochemical plating on the metal anode. Therefore, the development of strategies that can effectively change the coordination structure of Al^{3+} is the key to improving the CE of Al stripping/plating. Finally, the current strategy of increasing the concentration of salt will lead to an increase in the cost of ARAMBs. Therefore, it is also important to further develop modification strategies at low concentrations to meet cost requirements.

3) Unveiling the ambiguous reaction mechanism of electrodes and interfaces. Given that various ions are present

© 2025 The Author(s). Co-published by the Institute of Process Engineering, Chinese Academy of Sciences and the Royal Society of Chemistry

Ind. Chem. Mater., 2025, **3**, 7–30 | **25**

in the aqueous electrolyte, the cathode can react with H^+, Al^{3+}, $Al(OTF)_2^{2+}$, $Al(H_2O)_6^{3+}$, $Al_2Cl_7^-$, etc. during the discharge process, making it difficult to design stable cathodes for ARAMBs. Simultaneously, the presence of various ions also makes it difficult to clearly study the mechanism of the electrochemical deposition of Al. In combination with advanced operando characterizations and theoretical calculations, we expect that the reason for different reaction mechanisms at electrodes and interfaces with various types of cathode materials and electrolytes can be illustrated, thus providing fundamental principles for the future design of ARAMBs.

4) Evaluating the electrochemical performance of ARAMBs under practical conditions. Currently, the electrochemical tests of ARAMBs are usually performed under the conditions of coin cells or even three-electrode systems, in which most side reactions are ignored. Thus, by evaluating the behaviour under practical conditions, for example, low anode to cathode capacity ratio, high cathode loading, lean electrolytes, and high overall capacity (>1 Ah), we can better demonstrate whether the designed batteries are suitable for commercial applications. Through the simultaneous progress on the anode, electrolyte, and cathode, the overall electrochemical performance of ARAMBs can be further enhanced to satisfy the requirement of future energy storage/conversion systems.

Data availability statement

No primary research results, software or code have been included and no new data were generated or analysed as part of this review.

Conflicts of interest

The authors declare no conflict of interest.

Acknowledgements

References

1 B. Dunn, H. Kamath and J. M. Tarascon, Electrical energy storage for the grid: A battery of choices, *Science*, 2011, **334**, 928–935.

2 P. J. Heptonstall and R. J. K. Gross, A systematic review of the costs and impacts of integrating variable renewables into power grids, *Nat. Energy*, 2021, **6**, 72–83.

3 Z. X. Zhu, T. L. Jiang, M. Ali, Y. H. Meng, Y. Jin, Y. Cui and W. Chen, Rechargeable batteries for grid scale energy storage, *Chem. Rev.*, 2022, **122**, 16610–16751.

4 Z. Yang, J. Zhang, M. C. W. Kintner-Meyer, X. Lu, D. Choi, J. P. Lemmon and J. Liu, Electrochemical energy storage for green grid, *Chem. Rev.*, 2011, **111**, 3577–3613.

5 J. B. Goodenough, How we made the Li-ion rechargeable battery, *Nat. Electron.*, 2018, **1**, 204–204.

6 J. W. Choi and D. Aurbach, Promise and reality of post-lithium-ion batteries with high energy densities, *Nat. Rev. Mater.*, 2016, **1**, 16013.

7 S. Xin, X. Zhang, L. Wang, H. J. Yu, X. Chang, Y. M. Zhao, Q. H. Meng, P. Xu, C. Z. Zhao, J. H. Chen, H. C. Lu, X. R. Kong, J. L. Wang, K. Chen, G. Huang, X. B. Zhang, Y. Su, Y. Xiao, S. L. Chou, S. L. Zhang, Z. P. Guo, A. B. Du, G. L. Cui, G. J. Yang, Q. Zhao, L. B. Dong, D. Zhou, F. Y. Kang, H. Hong, C. Y. Zhi, Z. Z. Yuan, X. F. Li, Y. F. Mo, Y. Z. Zhu, D. F. Yu, X. C. Lei, J. X. Zhao, J. Y. Wang, D. Su, Y. G. Guo, Q. Zhang, J. Chen and L. J. Wan, Roadmap for rechargeable batteries: Present and beyond, *Sci. China: Chem.*, 2023, **67**, 13–42.

8 N. Yabuuchi, K. Kubota, M. Dahbi and S. Komaba, Research development on sodium-Ion batteries, *Chem. Rev.*, 2014, **114**, 11636–11682.

9 Y.-F. Zhu, Y. Xiao, S.-X. Dou, Y.-M. Kang and S.-L. Chou, Spinel/Post-spinel engineering on layered oxide cathodes for sodium-ion batteries, *eScience*, 2021, **1**, 13–27.

10 J. Muldoon, C. B. Bucur and T. Gregory, Quest for nonaqueous multivalent secondary batteries: Magnesium and beyond, *Chem. Rev.*, 2014, **114**, 11683–11720.

11 D. L. Chao, W. H. Zhou, F. X. Xie, C. Ye, H. Li, M. Jaroniec and S. Z. Qiao, Roadmap for advanced aqueous batteries: From design of materials to applications, *Sci. Adv.*, 2020, **6**, eaba4098.

12 Q. Zhao, W. W. Huang, Z. Q. Luo, L. J. Liu, Y. Lu, Y. X. Li, L. Li, J. Y. Hu, H. Ma and J. Chen, High-capacity aqueous zinc batteries using sustainable quinone electrodes, *Sci. Adv.*, 2018, **4**, eaao1761.

13 L. Miao, Y. K. Lv, D. Z. Zhu, L. C. Li, L. H. Gan and M. X. Liu, Recent advances in zinc-ion hybrid energy storage: Coloring high-power capacitors with battery-level energy, *Chin. Chem. Lett.*, 2023, **34**, 107784.

14 Z. Cai, J. Wang and Y. Sun, Anode corrosion in aqueous Zn metal batteries, *eScience*, 2023, **3**, 100093.

15 J. Ren, H.-Y. Wu, W. Yan, P. Huang and C. Lai, Stable zinc anode by regulating the solvated shell and electrode–electrolyte interface with a sodium tartrate additive, *Ind. Chem. Mater.*, 2024, **2**, 328–339.

16 Y. Y. Liu, G. J. He, H. Jiang, I. P. Parkin, P. R. Shearing and D. J. L. Brett, Cathode design for aqueous rechargeable multivalent ion batteries: Challenges and opportunities, *Adv. Funct. Mater.*, 2021, **31**, 2010445.

17 Q. Li and N. J. Bjerrum, Aluminum as anode for energy storage and conversion: A review, *J. Power Sources*, 2002, **110**, 1–10.

18 Y. Liu, Q. Sun, W. Li, K. R. Adair, J. Li and X. Sun, A comprehensive review on recent progress in aluminum–air batteries, *Green Energy Environ.*, 2017, **2**, 246–277.

19 D. Peramunage and S. Licht, A solid sulfur cathode for aqueous batteries, *Science*, 1993, **261**, 1029–1032.

20 D. Peramunage, R. Dillon and S. Licht, Investigation of a novel aqueous aluminum/sulfur battery, *J. Power Sources*, 1993, **45**, 311–323.

21 P. Ding, J. Zhang, N. Han, Y. Zhou, L. Jia and Y. Li, Simultaneous power generation and CO_2 valorization by aqueous Al–CO_2 batteries using nanostructured Bi_2S_3 as the cathode electrocatalyst, *J. Mater. Chem. A*, 2020, **8**, 12385–12390.

22 S. Zaromb, The use and behavior of aluminum anodes in alkaline primary batteries, *J. Electrochem. Soc.*, 1962, **109**, 1125.

23 N. Jayaprakash, S. K. Das and L. A. Archer, The rechargeable aluminum-ion battery, *Chem. Commun.*, 2011, **47**, 12610–12612.

24 M. C. Lin, M. Gong, B. G. Lu, Y. P. Wu, D. Y. Wang, M. Y. Guan, M. Angell, C. X. Chen, J. Yang, B. J. Hwang and H. J. Dai, An ultrafast rechargeable aluminium-ion battery, *Nature*, 2015, **520**, 324–328.

25 E. Faegh, B. Ng, D. Hayman and W. E. Mustain, Practical assessment of the performance of aluminium battery technologies, *Nat. Energy*, 2021, **6**, 21–29.

26 G. Wang, E. Dmitrieva, B. Kohn, U. Scheler, Y. Liu, V. Tkachova, L. Yang, Y. Fu, J. Ma, P. Zhang, F. Wang, J. Ge and X. Feng, An efficient rechargeable aluminium–amine battery working under quaternization chemistry, *Angew. Chem., Int. Ed.*, 2022, **61**, e202116194.

27 D. J. Kim, D.-J. Yoo, M. T. Otley, A. Prokofjevs, C. Pezzato, M. Owczarek, S. J. Lee, J. W. Choi and J. F. Stoddart, Rechargeable aluminium organic batteries, *Nat. Energy*, 2019, **4**, 51–59.

28 Z. Huang, X. Du, M. Ma, S. Wang, Y. Xie, Y. Meng, W. You and L. Xiong, Organic cathode materials for rechargeable aluminum-ion batteries, *ChemSusChem*, 2023, **16**, e202202358.

29 H. Chen, H. Y. Xu, S. Y. Wang, T. Q. Huang, J. B. Xi, S. Y. Cai, F. Guo, Z. Xu, W. W. Gao and C. Gao, Ultrafast all-climate aluminum-graphene battery with quarter-million cycle life, *Sci. Adv.*, 2017, **3**, eaao7233.

30 Z. J. Lin, M. L. Mao, C. X. Yang, Y. X. Tong, Q. H. Li, J. M. Yue, G. J. Yang, Q. H. Zhang, L. Hong, X. Q. Yu, L. Gu, Y. S. Hu, H. Li, X. J. Huang, L. M. Suo and L. Q. Chen, Amorphous anion-rich titanium polysulfides for aluminum-ion batteries, *Sci. Adv.*, 2021, **7**, eabg6314.

31 Q. Pang, J. Meng, S. Gupta, X. Hong, C. Y. Kwok, J. Zhao, Y. Jin, L. Xu, O. Karahan, Z. Wang, S. Toll, L. Mai, L. F. Nazar, M. Balasubramanian, B. Narayanan and D. R. Sadoway, Fast-charging aluminium–chalcogen batteries resistant to dendritic shorting, *Nature*, 2022, **608**, 704–711.

32 C. Xu, T. Diemant, A. Mariani, M. E. Di Pietro, A. Mele, X. Liu and S. Passerini, Locally concentrated ionic liquid electrolytes for wide-temperature-range aluminum-sulfur batteries, *Angew. Chem., Int. Ed.*, 2024, **63**, e202318204.

33 C. Xu, M. Zarrabeitia, Y. Li, J. Biskupek, U. Kaiser, X. Liu and S. Passerini, Three-dimensional nitrogen-doped carbonaceous networks anchored with cobalt as separator modification layers for low-polarization and long-lifespan aluminum–sulfur batteries, *ACS Nano*, 2023, **17**, 25234–25242.

34 Y. Guo, W. Wang, H. Lei, M. Wang and S. Jiao, Alternate storage of opposite charges in multisites for high-energy-density Al–MOF batteries, *Adv. Mater.*, 2022, **34**, 2110109.

35 Q. Zhao, J. X. Zheng, Y. Deng and L. Archer, Regulating the growth of aluminum electrodeposits: towards anode-free Al batteries, *J. Mater. Chem. A*, 2020, **8**, 23231–23238.

36 Y. H. Heo, J. Lee, S. Ha, J. Chan Hyun, D. H. Kang, J. Yoon, H. S. Kim, Y. Choi, Y. Chan Kang, H.-J. Jin, S. J. Kim and Y. S. Yun, 3D-structured bifunctional MXene paper electrodes for protection and activation of Al metal anodes, *J. Mater. Chem. A*, 2023, **11**, 14380–14389.

37 J. Yoon, S. Moon, S. Ha, H.-K. Lim, H.-J. Jin and Y. S. Yun, Nanoconfinement effect of nanoporous carbon electrodes for ionic liquid-based aluminum metal anode, *J. Energy Chem.*, 2022, **74**, 121–127.

38 S. Ha, J. C. Hyun, J. H. Kwak, H.-D. Lim, B. S. Youn, S. Cho, H.-J. Jin, H.-K. Lim, S. M. Lee and Y. S. Yun, Waste-induced pyrolytic carbon nanotube forest as a catalytic host electrode for high-performance aluminum metal anodes, *Chem. Eng. J.*, 2022, **437**, 135416.

39 J. Y. Shi, J. Zhang and J. Guo, Avoiding pitfalls in rechargeable aluminum batteries research, *ACS Energy Lett.*, 2019, **4**, 2124–2129.

40 X. Ma, J. Yu, Y. Hu, J. Texter and F. Yan, Ionic liquid/poly(ionic liquid)-based electrolytes for lithium batteries, *Ind. Chem. Mater.*, 2023, **1**, 39–59.

41 G. A. Elia, K. Marquardt, K. Hoeppner, S. Fantini, R. Y. Lin, E. Knipping, W. Peters, J. F. Drillet, S. Passerini and R. Hahn, An overview and future perspectives of aluminum batteries, *Adv. Mater.*, 2016, **28**, 7564–7579.

42 Q. Zhao, S. Stalin and L. A. Archer, Stabilizing metal battery anodes through the design of solid electrolyte interphases, *Joule*, 2021, **5**, 1119–1142.

43 S. Liu, J. J. Hu, N. Yan, G. Pan, G. Li and X. Gao, Aluminum storage behavior of anatase TiO_2 nanotube arrays in aqueous solution for aluminum ion batteries, *Energy Environ. Sci.*, 2012, **5**, 9743–9746.

44 W. H. Zuo, W. H. Zhu, D. F. Zhao, Y. F. Sun, Y. Y. Li, J. P. Liu and X. W. Lou, Bismuth oxide: A versatile high-capacity electrode material for rechargeable aqueous metal-ion batteries, *Energy Environ. Sci.*, 2016, **9**, 2881–2891.

45 T. Koketsu, J. W. Ma, B. J. Morgan, M. Body, C. Legein, W. Dachraoui, M. Giannini, A. Demortière, M. Salanne, F. Dardoize, H. Groult, O. J. Borkiewicz, K. Chapman, P. Strasser and D. Dambournet, Reversible magnesium and aluminium ions insertion in cation-deficient anatase TiO, *Nat. Mater.*, 2017, **16**, 1142–1148.

46 H. Y. Ma, H. W. Chen, Y. J. Hu, B. J. Yang, J. Z. Feng, Y. T. Xu, Y. L. Sun, H. H. Cheng, C. Li, X. B. Yan and L. T. Qu, Aqueous rocking-chair aluminum-ion capacitors enabled by a self-adaptive electrochemical pore-structure remolding approach, *Energy Environ. Sci.*, 2022, **15**, 1131–1143.

© 2025 The Author(s). Co-published by the Institute of Process Engineering, Chinese Academy of Sciences and the Royal Society of Chemistry

Ind. Chem. Mater., 2025, **3**, 7–30 | **27**

47 H. Yu, C. Lv, C. Yan and G. Yu, Interface engineering for aqueous aluminum metal batteries: Current progresses and future prospects, *Small Methods*, 2023, 2300758.

48 Q. Zhao, M. J. Zachman, W. I. Al Sadat, J. X. Zheng, L. F. Kourkoutis and L. Archer, Solid electrolyte interphases for high-energy aqueous aluminum electrochemical cells, *Sci. Adv.*, 2018, **4**, eaau8131.

49 Q. Zhao, L. Liu, J. Yin, J. Zheng, D. Zhang, J. Chen and L. A. Archer, Proton intercalation/de-intercalation dynamics in vanadium oxides for aqueous aluminum electrochemical cells, *Angew. Chem.*, 2020, **59**, 3048–3052.

50 X. B. Cheng, R. Zhang, C. Z. Zhao and Q. Zhang, Toward safe lithium metal anode in rechargeable batteries: A review, *Chem. Rev.*, 2017, **117**, 10403–10473.

51 S. Kumar, V. Verma, H. Arora, W. Manalastas and M. Srinivasan, Rechargeable Al-metal aqueous battery using NaMnHCF as a cathode: Investigating the role of coated-Al anode treatments for superior battery cycling performance, *ACS Appl. Energy Mater.*, 2020, **3**, 8627–8635.

52 D. Wang, H. Lv, T. Hussain, Q. Yang, G. Liang, Y. Zhao, L. Ma, Q. Li, H. Li, B. Dong, T. Kaewmaraya and C. Zhi, A manganese hexacyanoferrate framework with enlarged ion tunnels and two-species redox reaction for aqueous Al-ion batteries, *Nano Energy*, 2021, **84**, 105945.

53 Y. Li, L. Liu, Y. Lu, R. Shi, Y. Ma, Z. Yan, K. Zhang and J. Chen, High-energy-density quinone-based electrodes with $[Al(OTF)]^{2+}$ storage mechanism for rechargeable aqueous aluminum batteries, *Adv. Funct. Mater.*, 2021, **31**, 2102063.

54 J. Smajic, A. Alazmi, N. Wehbe and P. M. F. J. Costa, Electrode–electrolyte interactions in an aqueous aluminum–carbon rechargeable battery system, *Nanomaterials*, 2021, **11**, 3235.

55 Y. Cai, S. Kumar, R. Chua, V. Verma, D. Yuan, Z. K. Kou, H. Ren, H. Arora and M. Srinivasan, Bronze-type vanadium dioxide holey nanobelts as high performing cathode material for aqueous aluminium-ion batteries, *J. Mater. Chem. A*, 2020, **8**, 12716–12722.

56 R. F. Bai, J. Yang, G. J. Li, J. Y. Luo and W. J. Tang, Rechargeable aqueous aluminum-FeFe(CN)$_6$ battery with artificial interphase through deep eutectic solution, *Energy Storage Mater.*, 2021, **41**, 41–50.

57 T. Dong, K. L. Ng, Y. J. Wang, O. Voznyy and G. Azimi, Solid electrolyte interphase engineering for aqueous aluminum metal batteries: A critical evaluation, *Adv. Energy Mater.*, 2021, **11**, 2100077.

58 S. Kumar, T. Salim, V. Verma, W. Manalastas and M. Srinivasan, Enabling Al-metal anodes for aqueous electrochemical cells by using low-cost eutectic mixtures as artificial protective interphase, *Chem. Eng. J.*, 2022, **435**, 134742.

59 Q. F. Hao, F. Chen, X. T. Chen, Q. H. Meng, Y. Qi and N. Li, Bi-functional poly(vinylidene difluoride) coated Al anodes for highly rechargeable aqueous Al-ion batteries, *Electrochim. Acta*, 2022, **421**, 140495.

60 C. S. Yan, C. D. Lv, B. E. Jia, L. X. Zhong, X. Cao, X. L. Guo, H. J. Liu, W. J. Xu, D. B. Liu, L. Yang, J. W. Liu, H. H. Hng, W. Chen, L. Song, S. Z. Li, Z. Liu, Q. Y. Yan and G. H. Yu, Reversible Al metal anodes enabled by amorphization for aqueous aluminum batteries, *J. Am. Chem. Soc.*, 2022, **144**, 11444–11455.

61 Q. Ran, S. P. Zeng, M. H. Zhu, W. B. Wan, H. Meng, H. Shi, Z. Wen, X. Y. Lang and Q. Jiang, Uniformly MXene-grafted eutectic aluminum-cerium alloys as flexible and reversible anode materials for rechargeable aluminum-ion battery, *Adv. Funct. Mater.*, 2023, **33**, 2211271.

62 C. B. Breslin and W. M. Carroll, The electrochemical behaviour of aluminium activated by gallium in aqueous electrolytes, *Corros. Sci.*, 1992, **33**, 1735–1746.

63 B.-E. Jia, E. Hu, Z. Hu, J. J. Liew, Z. Hong, Y. Guo, M. Srinivasan, Q. Zhu, J. Xu, J. Chen, H. Pan and Q. Yan, Laminated tin–aluminum anodes to build practical aqueous aluminum batteries, *Energy Storage Mater.*, 2024, **65**, 103141.

64 C. S. Yan, C. Lv, L. G. Wang, W. Cui, L. Y. Zhang, K. N. Dinh, H. T. Tan, C. Wu, T. P. Wu, Y. Ren, J. Q. Chen, Z. Liu, M. Srinivasan, X. H. Rui, Q. Y. Yan and G. H. Yu, Architecting a stable high-energy aqueous Al-ion battery, *J. Am. Chem. Soc.*, 2020, **142**, 15295–15304.

65 J. He, X. Shi, C. Wang, H. Zhang, X. Liu, Z. Yang and X. Lu, A quinone electrode with reversible phase conversion for long-life rechargeable aqueous aluminum–metal batteries, *Chem. Commun.*, 2021, **57**, 6931–6934.

66 Q. Ran, H. Shi, H. Meng, S. P. Zeng, W. B. Wan, W. Zhang, Z. Wen, X. Y. Lang and Q. Jiang, Aluminum-copper alloy anode materials for high-energy aqueous aluminum batteries, *Nat. Commun.*, 2022, **13**, 576.

67 S. Arshadi Rastabi, G. Razaz, M. Hummelgård, T. Carlberg, N. Blomquist, J. Örtegren and H. Olin, Metallurgical investigation of aluminum anode behavior in water-in-salt electrolyte for aqueous aluminum batteries, *J. Power Sources*, 2022, **523**, 231066.

68 C. Wu, S. C. Gu, Q. H. Zhang, Y. Bai, M. Li, Y. F. Yuan, H. L. Wang, X. Y. Liu, Y. X. Yuan, N. Zhu, F. Wu, H. Li, L. Gu and J. Lu, Electrochemically activated spinel manganese oxide for rechargeable aqueous aluminum battery, *Nat. Commun.*, 2019, **10**, 73.

69 A. X. Zhou, L. W. Jiang, J. M. Yue, Y. X. Tong, Q. Q. Zhang, Z. J. Lin, B. H. Liu, C. Wu, L. M. Suo, Y. S. Hu, H. Li and L. Q. Chen, Water-in-salt electrolyte promotes high-capacity FeFe(CN)$_6$ cathode for aqueous Al-ion battery, *ACS Appl. Mater. Interfaces*, 2019, **11**, 41356–41362.

70 Y. Gao, H. Yang, X. Wang, Y. Bai, N. Zhu, S. Guo, L. Suo, H. Li, H. Xu and C. Wu, The compensation effect mechanism of Fe–Ni mixed prussian blue analogues in aqueous rechargeable aluminum-ion batteries, *ChemSusChem*, 2020, **13**, 732–740.

71 W. D. Pan, Y. F. Wang, Y. G. Zhang, H. Y. H. Kwok, M. Y. Wu, X. L. Zhao and D. Y. C. Leung, A low-cost and dendrite-free rechargeable aluminium-ion battery with superior performance, *J. Mater. Chem. A*, 2019, **7**, 17420–17425.

72 Y. Xu, J. L. Ma, T. L. Jiang, H. H. Ding, W. P. Wang, M. M. Wang, X. H. Zheng, J. F. Sun, Y. Yuan, M. Y. Chuai, N.

Chen, Z. Y. Li, H. L. Hu and W. Chen, Tuning electrolyte solvation structures to enable stable aqueous Al/MnO₂ battery, *Energy Storage Mater.*, 2022, **47**, 113–121.

73 W. Pan, J. Mao, Y. Wang, X. Zhao, K. W. Leong, S. Luo, Y. Chen and D. Y. C. Leung, High-performance MnO₂/Al battery with In Situ electrochemically reformed AlₓMnO₂ nanosphere cathode, *Small Methods*, 2021, **5**, 2100491.

74 Q. Sun, L. Chai, S. Chen, W. Zhang, H. Y. Yang and Z. Li, Dual-salt mixed electrolyte for high performance aqueous aluminum batteries, *ACS Appl. Mater. Interfaces*, 2024, **16**, 10061–10069.

75 Y. N. Gao, Y. Li, H. Y. Yang, L. M. Zheng, Y. Bai and C. Wu, Bi-salt electrolyte for aqueous rechargeable aluminum battery, *J. Energy Chem.*, 2022, **67**, 613–620.

76 W. Tang, L. Deng, L. Guo, S. Zhou, Q. Jiang and J. Luo, Reversible aqueous aluminum metal batteries enabled by a water-in-salt electrolyte, *Green Energy Environ.*, 2024, **9**, 1183–1191.

77 X. Yang, H. Gu, Q. Sun, W. Zhang and Z. Li, Synergistic co-embedding of metal ions and hydrogen protons for high stability double salt aqueous aluminum battery, *Energy Storage Mater.*, 2023, **61**, 102917.

78 X. J. Li, Y. C. Tang, C. A. Li, H. M. Lv, H. D. Fan, W. L. Wang, T. H. Cai, Y. P. Cui, W. Xing, Z. F. Yan, C. Y. Zhi and H. F. Li, Relieving hydrogen evolution and anodic corrosion of aqueous aluminum batteries with hybrid electrolytes, *J. Mater. Chem. A*, 2022, **10**, 4739–4748.

79 Z. C. Zhao, Z. H. Zhang, T. Xu, W. B. Wang, B. F. Wang and X. B. Yu, Solvation structure regulation for highly reversible aqueous Al metal batteries, *J. Am. Chem. Soc.*, 2024, **146**, 2257–2266.

80 Z. Hu, Y. Guo, H. Jin, H. Ji and L.-J. Wan, A rechargeable aqueous aluminum–sulfur battery through acid activation in water-in-salt electrolyte, *Chem. Commun.*, 2020, **56**, 2023–2026.

81 H. Lv, S. Yang, C. Li, C. Han, Y. Tang, X. Li, W. Wang, H. Li and C. Zhi, Suppressing passivation layer of Al anode in aqueous electrolytes by complexation of H₂PO₄⁻ to Al³⁺ and an electrochromic Al ion battery, *Energy Storage Mater.*, 2021, **39**, 412–418.

82 M. Xia, H. Fu, K. Lin, A. M. Rao, L. Cha, H. Liu, J. Zhou, C. Wang and B. Lu, Hydrogen-bond regulation in organic/aqueous hybrid electrolyte for safe and high-voltage K-ion batteries, *Energy Environ. Sci.*, 2024, **17**, 1255–1265.

83 R. Tao, H. Fu, C. Gao, L. Fan, E. Xie, W. Lyu, J. Zhou and B. Lu, Tailoring interface to boost the high-performance aqueous Al ion batteries, *Adv. Funct. Mater.*, 2023, **33**, 2303072.

84 X. Ma, H. Fu, J. Shen, D. Zhang, J. Zhou, C. Tong, A. M. Rao, J. Zhou, L. Fan and B. Lu, Green ether electrolytes for sustainable high-voltage potassium ion batteries, *Angew. Chem., Int. Ed.*, 2023, **62**, e202312973.

85 Q. Pang, S. Yang, X. Yu, W. He, S. Zhang, Y. Tian, M. Xing, Y. Fu and X. Luo, Realizing reversible storage of trivalent aluminum ions using VOPO₄·2H₂O nanosheets as cathode material in aqueous aluminum metal batteries, *J. Alloys Compd.*, 2021, **885**, 161008.

86 S. Kumar, R. Satish, V. Verma, H. Ren, P. Kidkhunthod, W. Manalastas and M. Srinivasan, Investigating FeVO₄ as a cathode material for aqueous aluminum-ion battery, *J. Power Sources*, 2019, **426**, 151–161.

87 M. Tian, R. H. Li, C. F. Liu, D. H. Long and G. Z. Cao, Aqueous Al-ion supercapacitor with V₂O₅ mesoporous carbon electrodes, *ACS Appl. Mater. Interfaces*, 2019, **11**, 15573–15580.

88 R. Liu, J. Liu, Y. Li, C. Zhang and H. Li, Aqueous aluminum-ion batteries based on layered NH₄V₄O₁₀ nanosheets as cathode, *Solid State Sci.*, 2023, **145**, 107315.

89 S. Nandi, Y. Yan, X. Yuan, C. Wang, X. He, Y. Li and S. K. Das, Vanadyl ethylene glycolate: A novel organic-inorganic electrode material for rechargeable aqueous aluminum-ion battery, *Solid State Ionics*, 2023, **389**, 116085.

90 S. He, J. Wang, X. Zhang, J. Chen, Z. Wang, T. Yang, Z. Liu, Y. Liang, B. Wang, S. Liu, L. Zhang, J. Huang, J. Huang, L. A. O'Dell and H. Yu, A High-energy aqueous aluminum-manganese battery, *Adv. Funct. Mater.*, 2019, **29**, 1905228.

91 R. C. Li, C. H. Xu, X. B. Wu, J. L. Zhang, X. Yuan, F. Wang, Q. R. Yao, M. S. Balogun, Z. G. Lu and J. Q. Deng, Aluminum-ion storage reversibility in a novel spinel Al₂/₃Li₁/₃Mn₂O₄ cathode for aqueous rechargeable aluminum batteries, *Energy Storage Mater.*, 2022, **53**, 514–522.

92 J. Yang, W. Gong and F. Geng, Defect modulation in cobalt manganese oxide sheets for stable and high-energy aqueous aluminum-ion batteries, *Adv. Funct. Mater.*, 2023, **33**, 2301202.

93 W. J. Huang, K. Zhang, B. Yuan, L. C. Yang and M. Zhu, Predominant intercalation of H⁺ enables ultrahigh rate capability of oxygen deficient MoO₃ for aqueous Al-ion batteries, *Energy Storage Mater.*, 2022, **50**, 152–160.

94 C. Huang, Z. Jiang, F. Liu, W. Li, Q. Liang, Z. Zhao, X. Ge, K. Song, L. Zheng, X. Zhou, S. Qiao, W. Zhang and W. Zheng, Oxygen vacancies boosted hydronium intercalation: A paradigm shift in aluminum-based batteries, *Angew. Chem., Int. Ed.*, 2024, **63**, e202405592.

95 S. Nandi, Y. C. Yan, X. T. Yuan, C. Z. Wang, X. M. He, Y. Z. Li and S. K. Das, Investigation of reversible metal ion (Li⁺, Na⁺, Mg²⁺, Al³⁺) insertion in MoTe₂ for rechargeable aqueous batteries, *Phys. Chem. Chem. Phys.*, 2023, **25**, 13833–13837.

96 Z. Li, K. Xiang, W. Xing, W. C. Carter and Y.-M. Chiang, Reversible aluminum-ion intercalation in prussian blue analogs and demonstration of a high-power aluminum-ion asymmetric capacitor, *Adv. Energy Mater.*, 2014, **5**, 1401410.

97 S. Liu, G. L. Pan, G. R. Li and X. P. Gao, Copper hexacyanoferrate nanoparticles as cathode material for aqueous Al-ion batteries, *J. Mater. Chem. A*, 2015, **3**, 959–962.

© 2025 The Author(s). Co-published by the Institute of Process Engineering, Chinese Academy of Sciences and the Royal Society of Chemistry

Ind. Chem. Mater., 2025, **3**, 7–30 | 29

View Article Online

Industrial Chemistry & Materials

98 X. Li, A. Wu, C. Gao, Z. Li and S. W. Lee, Copper hexacyanoferrate as a long-life cathode for aqueous aluminum ion batteries, *Mater. Today Energy*, 2023, **31**, 101205.

99 Y. Ru, S. Zheng, H. Xue and H. Pang, Potassium cobalt hexacyanoferrate nanocubic assemblies for high-performance aqueous aluminum ion batteries, *Chem. Eng. J.*, 2020, **382**, 122853.

100 A. Zhao, W. Chang, Y. Xiao and N. Peng, Construction of cobalt hexacyanoferrate multivoid nanoframes as efficient aqueous aluminum ion batteries, *J. Alloys Compd.*, 2024, **976**, 173101.

101 X. Yuan, X. Yuan, S. Zhang, P. Chen, X. Wu, J. Ye, L. Liu, L. Fu, T. Wang, K. I. Ozoemena and Y. Wu, An aqueous rechargeable Al-ion battery based on cobalt hexacyanoferrate and Al metal, *Adv. Energy Mater.*, 2023, **14**, 2302712.

102 W. Pan, Y. Zhao, J. Mao, Y. Wang, X. Zhao, K. W. Leong, S. Luo, X. Liu, H. Wang, J. Xuan, S. Yang, Y. Chen and D. Y. C. Leung, High-energy SWCNT cathode for aqueous Al-ion battery boosted by multi-ion intercalation chemistry, *Adv. Energy Mater.*, 2021, **11**, 2101514.

103 J. Smajic, B. E. Hasanov, A. Alazmi, A. H. Emwas, N. Wehbe, A. Genovese, A. El Labban and P. M. F. J. Costa, Aqueous aluminum-carbon rechargeable batteries, *Adv. Mater. Interfaces*, 2021, **9**, 2101733.

104 B. B. Yang, Y. K. Wang, H. F. Bian, Y. L. Zhang, Y. Y. Du, H. B. Lu and D. Bin, A rocking-chair aqueous aluminum-ion battery based on an organic/inorganic electrode, *Chem. Commun.*, 2023, **59**, 8246–8249.

105 J. Su, M. Zhang, H. Tian, M. Han, Z. Sun, K. Du, F. Cui, J. Li, W. Huang and Y. Hu, Synergistic π-conjugation organic cathode for ultra-stable aqueous aluminum batteries, *Small*, 2024, DOI: **10.1002/smll.202312086**.

106 J. C. Chen, Q. N. Zhu, L. Jiang, R. Y. Liu, Y. Yang, M. Y. Tang, J. W. Wang, H. Wang and L. Guo, Rechargeable aqueous aluminum organic batteries, *Angew. Chem., Int. Ed.*, 2021, **60**, 5794–5799.

107 W. Wang, S. Zhang, L. Zhang, R. Wang, Q. Ma, H. Li, J. Hao, T. Zhou, J. Mao and C. Zhang, Electropolymerized bipolar poly(2,3-diaminophenazine) cathode for high-performance aqueous Al-ion batteries with an extended temperature range of −20 to 45 °C, *Adv. Mater.*, 2024, **36**, 2400642.

108 S. Jiang, Y. Xie, Y. Xie, L.-J. Yu, X. Yan, F.-G. Zhao, C. J. Mudugamuwa, M. L. Coote, Z. Jia and K. Zhang, Lewis acid-induced reversible disproportionation of TEMPO enables aqueous aluminum radical batteries, *J. Am. Chem. Soc.*, 2023, **145**, 14519–14528.

109 J. Joseph, J. Nerkar, C. Tang, A. Du, A. P. O'Mullane and K. Ostrikov, Reversible intercalation of multivalent Al^{3+} ions into potassium-rich cryptomelane nanowires for aqueous rechargeable Al-ion batteries, *ChemSusChem*, 2019, **12**, 3753–3760.

110 H. Meng, Q. Ran, M. H. Zhu, Q. Z. Zhao, G. F. Han, T. H. Wang, Z. Wen, X. Y. Lang and Q. Jiang, Benzoquinone-lubricated intercalation in manganese oxide for high-capacity and high-rate aqueous aluminum-ion battery, *Small*, 2024, **20**, 2310722.

111 J. Zheng, D. W. Li, Z. M. Feng, Y. Wang and T. Sun, Preintercalated copper hexacyanoferrate as a long-time cycle cathode material for aqueous aluminum-ion batteries, *ACS Sustainable Chem. Eng.*, 2023, **11**, 6280–6291.

112 Y. Ru, S. S. Zheng, H. G. Xue and H. Pang, Potassium cobalt hexacyanoferrate nanocubic assemblies for high-performance aqueous aluminum ion batteries, *Chem. Eng. J.*, 2020, **382**, 122853.